ΔE

$\Delta E = g\beta B_0$

Absorption

$B_0 \longrightarrow$

1st Derivative

Electron Paramagnetic Resonance Theory

E. Duin

1.   Basic EPR Theory

1.1   Introduction

This course manual will provide the reader with a basic understanding needed to be able to get useful information using the technique of electron paramagnetic resonance (EPR) spectroscopy.

EPR spectroscopy is similar to any other technique that depends on the absorption of electromagnetic radiation. A molecule or atom has discrete (or separate) states, each with a corresponding energy. Spectroscopy is the measurement and interpretation of the energy differences between the atomic or molecular states. With knowledge of these energy differences, you gain insight into the identity, structure, and dynamics of the sample under study.

We can measure these energy differences, ΔE, because of an important relationship between ΔE and the absorption of electromagnetic radiation. According to Planck's law, electromagnetic radiation will be absorbed if:

$$\Delta E = h\nu, \tag{1}$$

where h is Planck's constant and ν is the frequency of the radiation. The absorption of energy causes a transition from a lower energy state to a higher energy state. In conventional spectroscopy, ν is varied or swept and the frequencies at which absorption occurs correspond to the energy differences of the states. (We shall see later that EPR differs slightly.) Typically, the frequencies vary from the megahertz range for NMR (Nuclear Magnetic Resonance) (AM, FM, and TV transmissions use electromagnetic radiation at these frequencies), through visible light, to ultraviolet light. Radiation in the gigahertz range (GHz) with a wavelength of a few cm (ca. 3 cm) is used for EPR experiments. Such radiation lies far outside the visible region: it is *microwave radiation* used in ordinary radar equipment and microwave ovens.

1.2   The Zeeman Effect

An isolated electron, all alone in space without any outside forces, still has an intrinsic angular momentum called "spin", $\bar{S}$. Because an electron is charged, the angular motion of this charged particle generates a magnetic field. In other words, the electron due to its charge and angular momentum, acts like a little bar magnet, or magnetic dipole, with a magnetic moment, $\bar{\mu}$.

Fig. 1: Free, unpaired electron in space: electron spin – magnetic moment

The energy differences studied in EPR spectroscopy are predominately due to the interaction of **unpaired** electrons in the sample with a magnetic field produced by a magnet in the laboratory. This effect is called the **Zeeman Effect**. The magnetic field, B_0, produces two energy levels for the magnetic moment, $\bar{\mu}$, of the electron. The unpaired electron will have a state of lowest energy when the moment of the electron is aligned with the magnetic field and a stage of highest energy when $\bar{\mu}$ is aligned against the magnetic field.
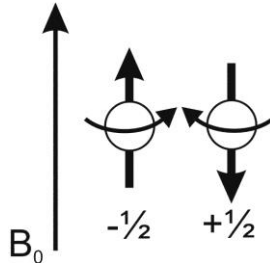

Fig. 2: Minimum and maximum energy orientations of $\bar{\mu}$ with respect to the magnetic field B_0

The two states are labeled by the projection of the electron spin, m_s, on the direction of the magnetic field. Because the electron is a spin ½ particle, the parallel state is designated as $m_s = -\frac{1}{2}$ and the antiparallel state is $m_s = +\frac{1}{2}$ (Figs. 2 and 3). The energy of each orientation is the product of μ and B_0. For an electron $\mu = m_s g_e \beta$, where β is a conversion constant called the Bohr magneton and g_e is the spectroscopic g-factor of the free electron and equals 2.0023192778 ($\approx$ 2.00). Therefore, the energies for an electron with $m_s = +\frac{1}{2}$ and $m_s = -\frac{1}{2}$ are, respectively

$$E_{1/2} = \tfrac{1}{2}\, g_e \beta B_0 \quad \text{and} \tag{2}$$

$$E_{-1/2} = -\tfrac{1}{2}\, g_e \beta B_0 \tag{3}$$

As a result there are two energy levels for the electron in a magnetic field.
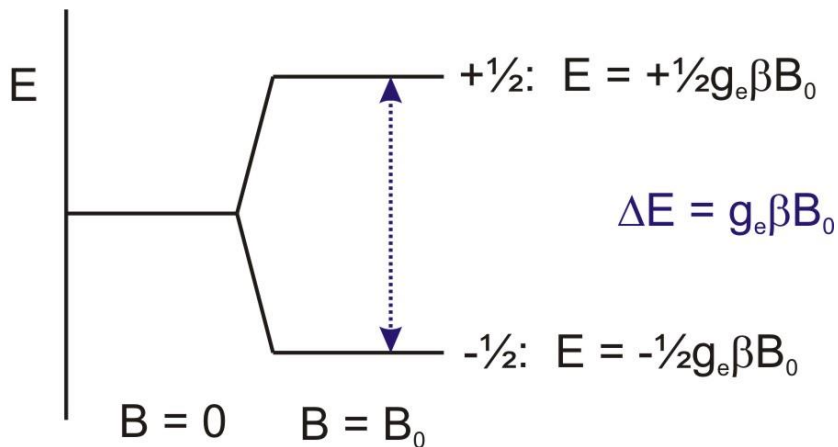

Fig. 3: Induction of the spin state energies as a function of the magnetic field B_0.

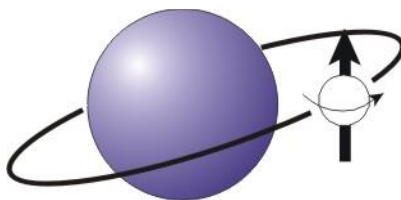## 1.3   Spin-Orbit Interaction

Fig. 4

When we take an electron in space with no outside forces on it and place it on to a molecule, its total angular momentum changes because, in addition to the intrinsic spin angular momentum ($\bar{S}$), it now also possesses some orbital angular momentum ($\bar{L}$). An electron with orbital angular momentum is in effect a circulating current, and so there is also a magnetic moment arising from the orbital angular momentum. These two magnetic moments interact, and the energy of this spin-orbit interaction depends on their relative orientations.

Electron in space

$$\bar{\mu} \propto g_e \bar{S} \tag{4}$$

Electron in a molecule

$$\bar{\mu} \propto g_e \bar{S} + \bar{L} \tag{5}$$

In general, the orbital angular momentum is approximately zero for an electron in the ground state (*s* electron). Interaction between the ground state and excited states, however, admixes small amounts of orbital angular momentum to the ground state: ***spin-orbit coupling contribution***.

$$\bar{\mu} \propto g_e \bar{S} + spin\text{-}orbit\ coupling\ contribution \tag{6}$$

It is common practice to assume that the spin-orbit coupling term is proportional to $\bar{S}$ which means we can simply combine both terms on the right and just change the value of g_e to g, or

$$\bar{\mu} \propto g\bar{S} \tag{7}$$

and

$$\Delta E = g\beta B_0 \tag{8}$$

The magnitude of the spin-orbit coupling contribution depends on the size of the nucleus containing the unpaired electron. Therefore, organic free radicals, with only H, O, C and N atoms, will have a small contribution from spin-orbit coupling, producing g factors very close to g_e while the g factors of much larger elements, such as metals, may be significantly different from g_e.

A simpler alternative way of thinking about the spin-orbit coupling is that a virtual observer on the electron would experience the nucleus (nuclei) as an orbiting positive charge producing a second magnetic field, δB, at the electron.

$$h\nu = g_e \beta (B_e + \delta B) \tag{9}$$

Since only the spectrometer value of B is known we can rewrite this as:

$$hv = (g_e + \delta g)\beta B = g\beta B \qquad (10)$$

The quantity '$g_e + \delta g$' or 'g' contains the chemical information on the nature of the bond between the electron and the molecule, the electronic structure of the molecule.

The value of g can be taken as a fingerprint of the molecule.

1.4   *g*-Factor

From the above discussion we can see that one parameter whose value we may wish to know is *g*. In an EPR spectrometer, a paramagnetic sample is placed in a large uniform magnetic field which, as shown above, splits the energy levels of the ground state by an amount *ΔE* where

$$\Delta E = g\beta B_0 = hv \qquad (11)$$

Since *β* is a constant and the magnitude of *B₀* can be measured, all we have to do to calculate *g* is determine the value of *ΔE*, the energy between the two spin levels. This is done by irradiating the sample with microwaves with a set frequency and sweeping the magnetic field (Fig. 5).
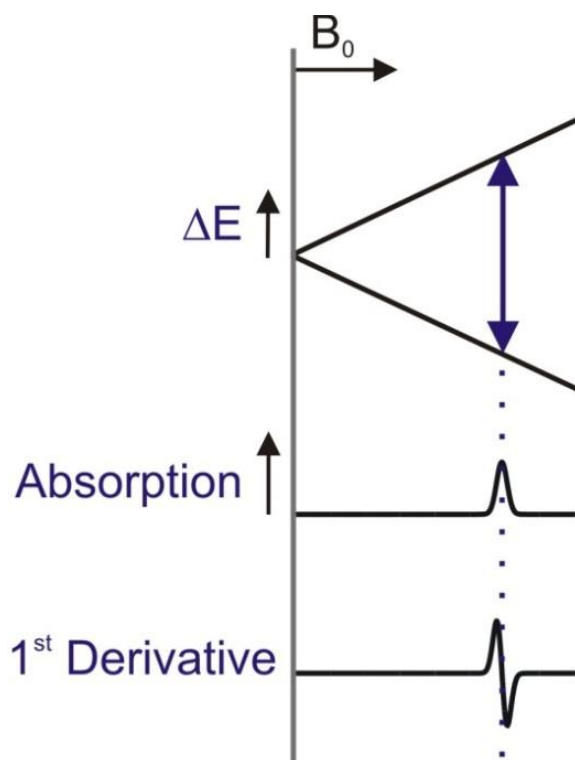

Fig. 5: The EPR experiment

Absorption of energies will occur when the condition in (11) is satisfied. The value of g can then be calculated from v (in GHz) and B_0 (in gauss) using,

$$g = \frac{hv}{\beta B_0} \tag{12}$$

or

$$g = 0.7145 \frac{v\ (MHz)}{B_0\ (Gauss)} \tag{13}$$

($h = 6.626 \cdot 10^{-34}$ J·s; $\beta = 9.274 \cdot 10^{-28}$ J·G^{-1})

Two facts are apparent from equations 2 and 3, equation 11 and the graph in Figure 5. Firstly, the two spin states have the same energy in the absence of a magnetic field. Secondly, the energies of the spin states diverge linearly as the magnetic field increases. These two facts have important consequences for spectroscopy:

1) Without a magnetic field, there is no energy difference to measure.
2) The measured energy difference depends linearly on the magnetic field

Because we can change the energy differences between the two spin states by varying the magnetic field strength, we have an alternative means to obtain spectra. We could apply a constant magnetic field and scan the frequency of the electromagnetic radiation as in conventional spectroscopy. Alternatively, we could keep the electromagnetic radiation frequency constant and scan the magnetic field. A peak in the absorption will occur when the magnetic field "tunes" to the two spin states so that their energy difference matches the energy of the radiation. This field is called the "field of resonance". A radiation source for radar waves produces only a very limited spectral region. In EPR such a source is called a klystron. A so-called X-band klystron has a spectral band width of about 8.8-9.6 GHz. This makes it impossible to continuously vary the wavelength similarly to optical spectroscopy. It is therefore necessary to vary the magnetic field, until the quantum of the radar waves fits between the field-induced energy levels.

1.5   Line Shape

In the above described EPR experiment we only looked at one molecule in one orientation in a magnetic field. The deviation of the measured g-factor from that of the free electron arises from spin-orbit coupling between the ground state and excited states. Because orbitals are oriented in the molecule, the magnitude of this mixing is direction dependent, or ***anisotropic***. In a low-viscosity solution, all of this anisotropy is averaged out. However, this is not the situation when all the paramagnetic molecules are in a fixed orientation, as in a single crystal. You would find that the g-factor of the EPR spectrum of a single crystal would change as you rotated the crystal in the spectrometer, due to g-factor anisotropy. For every paramagnetic molecule, there exists a unique axis system called the ***principal axis system***. The g-factors measured along these axes are called the principal g-factors and are labeled g_x, g_y and g_z.

Figure 6, shows as an example a molecule where the paramagnetic metal is coordinated by two equal ligands in the z-direction and four different but equal ligands in both the x- and y-directions. As a result the resulting g-factor will be different for the situations where the field B_0 is parallel to the z-axis or parallel to either the x- or y-axes.
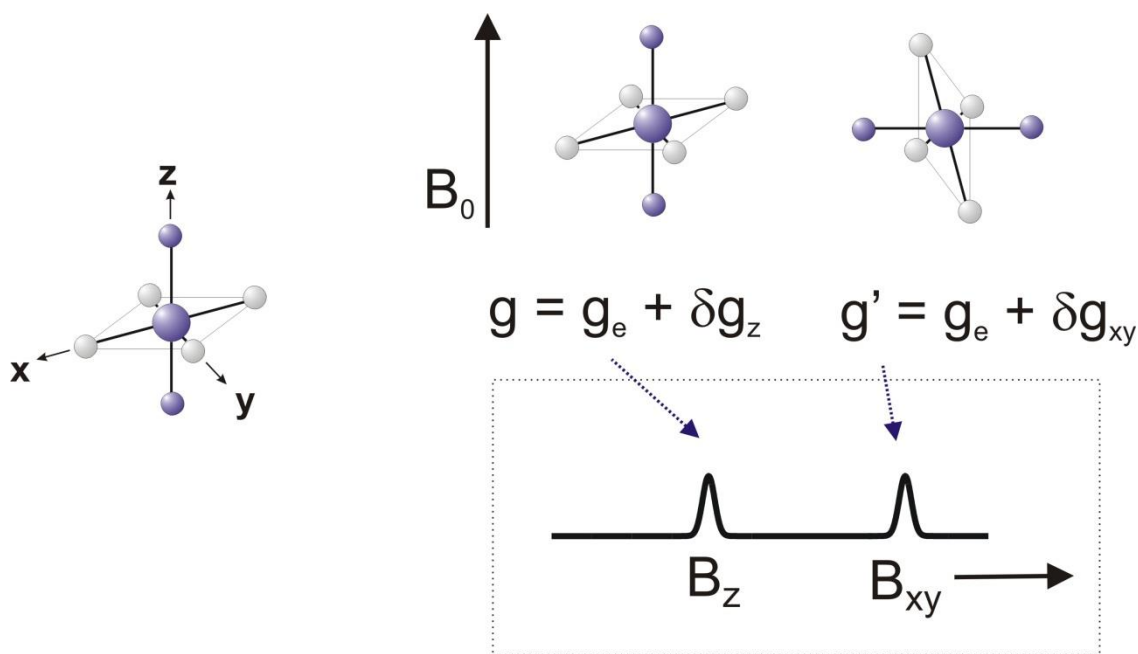

Fig. 6: Dependency of the g value on the oritentation of the molecules in the magnetic field.

Most EPR spectra of biological transition metals are recorded on frozen solution samples. In these samples, the paramagnets are neither aligned in a set direction, as in an oriented single crystal, nor are they rapidly rotating, as in a low-viscosity solution. The act of freezing fixes the molecules in all possible orientations. Therefore the spectrum of a frozen sample represents the summation of all possible orientations and is called a ***powder spectrum***. Note that to get the complete powder spectrum of a single crystal you would have to measure a spectrum for the crystal in all possible x-, y- and z-directions. Alternatively you could ground up the single crystal into an actual powder.
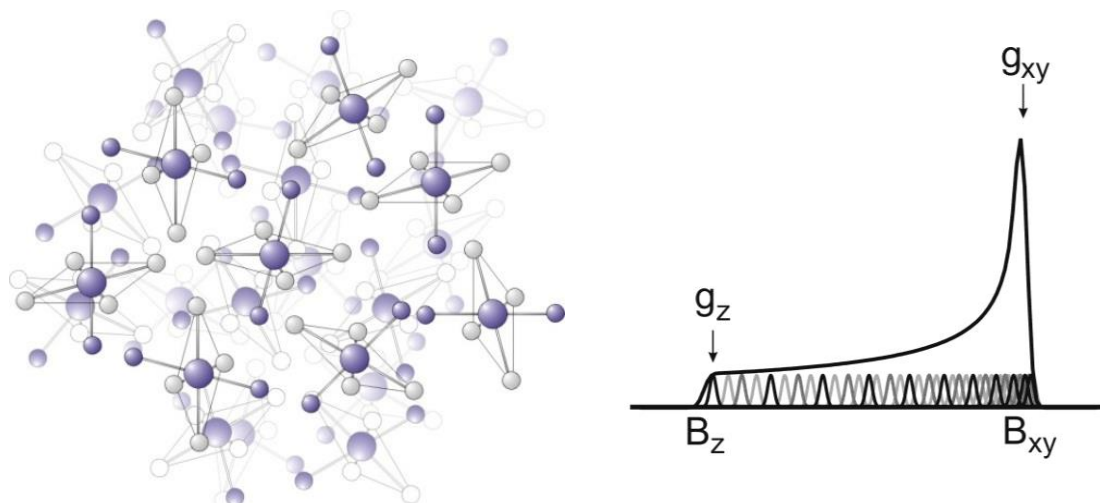
Fig. 7: A power spectrum is the sum of the spectra for all possible ortientations of the molecule

There is only one step left to understand the shape of spectra, measured with a frozen enzyme solution. It has to do with one of the **selection rules** in EPR, namely that only the magnetic moments from the sample in the direction of the external field (to be more precise: **perpendicular** to the direction of the magnetic field created by the microwaves) are detected. Imagine that a metal ion has a total symmetric environment, i.e. the electrons in the different *d*-orbitals have equal interactions in all directions: the orbital moment then is equal in all directions, so also the total magnetic moment is the same in all directions ($\mu_x = \mu_y = \mu_z$ so also $g_x = g_y = g_z$). Now if you put such an ion in an external field, it does not matter at all how you put it in: the magnitude of the total magnetic momentum in the direction of the external field will always be the same. This means that there is only one *g*-value and only one value of the external field where resonance occurs: $h\nu = g\beta B$. There will only be one absorption line (Fig. 8a).

Now suppose there is axial symmetry, such that the total magnetic moment in the *z*-direction is rather large. If you place such an ion in the external field, it does matter how you position it as shown in Figures 6 and 7. If you place it such that the *z*-direction is parallel to the external field *B*, the energy difference between the two energy levels for the electron will be $2\mu_z B$. Since we have assumed a large value of μ_z, we only need a small external field (B_z) to get resonance (Fig. 6). If we put our ion in the magnet with either the *x*-axis or the *y*-axis (or any other direction within the *xy*-plane) parallel to the external field, then the energy difference is $2\mu_{x,y}B$, As we have made $\mu_{x,y}$ small, we need a large field ($B_{x,y}$) for resonance (Fig. 6). If we rotate our ion from the 'z∥B' to the position 'z⊥B' (x,y-plane∥B), the total magnetic moment in the direction of the external field will decrease from μ_z to $\mu_{x,y}$. The one and only absorption line in the spectrum then moves from B_z to $B_{x,y}$.

In a frozen sample all orientations occur and consequently there are a large number of overlapping absorption lines starting at B_z and ending at $B_{x,y}$ (Fig. 7). What is detected is the sum of all these lines. It is simply a matter of statistics that our ion with its *x*- or *y*-direction parallel to *B* occurs much more frequently than one with its *z*-axis parallel to B. This is the reason that the total absorption in the *x,y*-direction is much larger than in the *z*-direction. This usually enables us to recognize those directions in a spectrum.

Fig. 8 shows the absorption and first-derivative spectra for three different classes of anisotropy. In the first class, called **isotropic**, all of the principal g-factors are the same (Fig. 8a). In the second class, called **axial**, there is a unique axis that differs from the other two ($g_x = g_y \neq g_z$) (Fig. 8b and c). This would have been the powder spectrum for our molecule shown in Fig. 6. The g-factor along the unique axis is said to be parallel with it, $g_z = g_{/\!/}$ while the remaining two axes are perpendicular to it, $g_{x,y} = g_\perp$. The last class, called **rhombic**, occurs when all the g-factors differ (Fig. 8d).
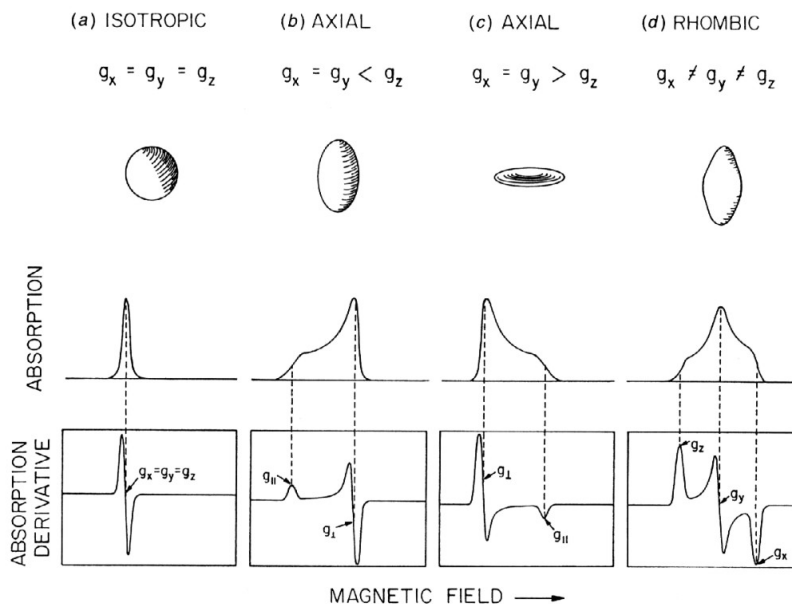

(a) ISOTROPIC (b) AXIAL (c) AXIAL (d) RHOMBIC

$g_x = g_y = g_z$ $g_x = g_y < g_z$ $g_x = g_y > g_z$ $g_x \neq g_y \neq g_z$

Fig. 8: Schematic representation of g tensor and the consequential EPR spectra. The upper solid bodies show the shapes associated with isotropic (a), axial (b, c) and rhombic (d) magnetic moments. Underneath are shown the absorption curves. The corresponding EPR derivative curves are shown on the bottom.

A more thorough way of describing the effect shown in Figure 6, is to define the angular dependency of the g-value. For this we first have to define the orientation of the magnetic field (a vector) with respect to the coordinates of the molecule (and vice versa). This can be done by defining two polar angles, θ and ϕ, where θ is the angle between the vector B and the molecular z-axis, and ϕ is the angle between the projection of B onto the xy-plane and the x-axis (Fig. 9).
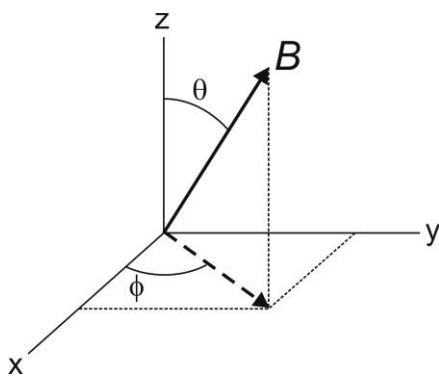

Fig. 9: Orientation of the magnetic field B with respect to the coordinates of the molecule.

In practice, however, so-called direction cosines are used:

$$l_x = \sin\theta\cos\varphi$$
$$l_y = \sin\theta\sin\varphi$$
$$l_z = \cos\theta$$

Now the anisotropic resonance condition for an $S = \frac{1}{2}$ system subject to the electronic Zeeman interaction can be defined as

$$B_{res} = \frac{h\upsilon}{g(l_x, l_y, l_z)\beta} \text{ with } g(l_x, l_y, l_z) = \sqrt{l_x^2 g_x^2 + l_y^2 g_y^2 + l_z^2 g_z^2} \tag{14}$$

Or in terms of the polar angles

$$g(\theta, \phi) = \sqrt{g_x^2 \sin^2\theta\cos^2\phi + g_y^2 \sin^2\theta\sin^2\phi + g_z^2\cos^2\theta} \tag{15}$$

Equation 15 can be simplified for axial spectra

$$g_{ax}(\theta) = \sqrt{g_{xy}^2 \sin^2\theta + g_z^2\cos^2\theta} \tag{16}$$

In which $g_\perp \equiv g_x \equiv g_y$, and $g_{/\!/} \equiv g_z$. Figure 10 shows a plot of θ and $g_{ax}(\theta)$ as a function of the resonance field B_{res}. Note that the resonance field B_{res} is relatively insensitive to change in orientation (here, in θ) for orientations of B near the molecular axes (here $\theta = 0$ or $\pi/2$)
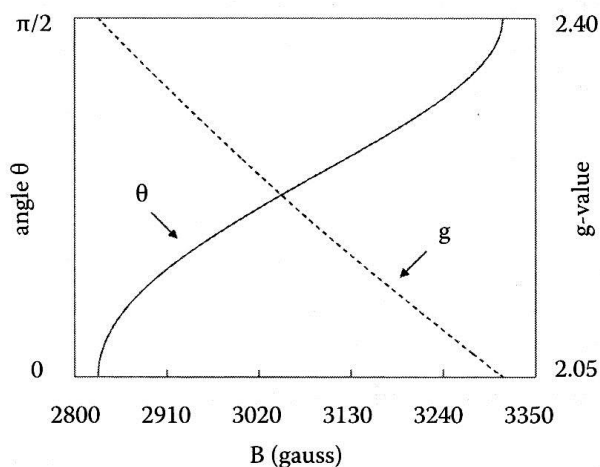

Fig. 10: Angular dependency of axial *g*-value. The angle θ between B_0 and the molecular *z*-axis and the axial *g*-value are plotted versus the resonance field for a typical tetragonal Cu(II) site with $g_{/\!/} = 2.40$ and $g_\perp = 2.05$: $\upsilon = 9500$ MHz.

As a result of this insensitivity, clear so-called turning-point features appear in the powder spectrum that closely correspond with the position of the *g*-values. Therefore the *g*-values can be read from the absorption-type spectra. For practical reasons (see chapter 2), the first derivative instead of the true absorption is recorded. In these types of spectra the *g*-values are very easy to recognize. This is

not the reason, however, that the first derivative is recorded. To improve the sensitivity of the EPR spectrometer, magnetic field modulation is used. In field modulation, the amplitude of the external field, B_0, is made to change by a small amount (~ 0.1-20 G) at a frequency of 100 kHz (other frequencies can also be used). Because the spectrometer is tuned to only detect signals that change amplitude as the field changes, the resultant signal appears as a first derivative (i.e., ΔSignal amplitude/ΔMagnetic field). The derivative spectra are characterized by those places where the first derivative of the absorption spectrum has its extreme values. In EPR spectra of simple S = ½ systems there are maximally 3 such places which correspond with the g-factors. The position of these 'lines' can be expressed in field units (Gauss, or Tesla (1 T = 10^4 G)), but it is better to use the so-called g-value. The field for resonance is not a unique "fingerprint" for identification of a compound because spectra can be acquired at several different frequencies using different klystrons. The g-factor, being independent of the microwave frequency, is much better for that purpose. Notice that high values of a g occur at low magnetic fields and vice versa. A list of fields for resonance for a g = 2 signal at microwave frequencies commonly available in EPR spectrometers is presented in Table 1.1.

Table 1.1: Field for resonance B_{res} for a g = 2 signal at selected microwave frequencies

Microwave Band	Frequency (GHz)	B_{res} (G)
L	1.1	392
S	3.0	1070
X	9.5	3389
Q	35	12485
W	90	32152
J	270	96458

An advantage of derivative spectroscopy is that it emphasizes rapidly-changing features of the spectrum, thus enhancing resolution. Note, however, that a slowly changing part of the spectrum has near zero slope, so in the derivative display there is "no intensity". This can be detected in the examples of the two types of axial spectra shown in Figure 8 (b and c). While the absorption spectrum clearly shows intensity between the $g_{\parallel}$ and $g_{\perp}$ values, the derivative spectrum is pretty much flat in between the peaks indicating the $g_{\parallel}$ and $g_{\perp}$ positions. This makes it sometimes difficult to estimate the concentration of EPR samples since a large part of the signal appears to be hidden. A typical mistake is too assign a larger intensity to an isotropic signal ($g_x = g_y = g_z$) while a broad axial or rhombic signal is viewed as having less intensity. An isotropic signal has all the signal intensity spread over a very small field region causing the signal to have a very large signal amplitude, while a broad axial or rhombic signal is spread over a larger field region causing the observed amplitude to decrease significantly.

1.6   Quantum Mechanical Description

A full quantum mechanical description of the spectroscopic EPR event is not possible due to the complexity of the systems under study. In particular the lack of symmetry in biological samples excludes the use of this aspect in simplifying the mathematical equations. Instead in Biomolecular EPR the concept of the **spin Hamiltonian** is used. This describes a system with an extremely simplified form of the **Schrödinger wave equation** that is a valid description *only* of the lowest electronic state of the molecule *plus* magnetic interactions. In this description the simplified operator, H_s, is the spin Hamiltonian, the simplified wave function, ψ_s, are the spin functions, and the eigenvalues E are the energy values of the ground state spin manifold.

$$H_s\psi_s = E\psi_s \tag{17}$$

For an isolated system with a single unpaired electron and no hyperfine interaction the only relevant interaction is the electronic Zeeman term, so the spin Hamiltonian is

$$H_s = \beta B(g_x l_x S_x + g_y l_y S_y + g_z l_z S_z) \tag{18}$$

A shorter way of writing this is

$$H_s = \beta B \bullet g \bullet S \tag{19}$$

Solving this we get the equation we saw earlier for the angular dependency of the *g*-value

$$hv = \sqrt{g_x^2 l_x^2 + g_y^2 l_y^2 + g_z^2 l_z^2}\ \beta B \tag{20}$$

More terms can be added to the Hamiltonian when needed as for example described in the next section where the effect of nuclear spin is introduced. The emphasis of this text (and the associated EPR course) is to get a practical understanding of EPR spectroscopy. A full quantum mechanical description is outside the scope of this text. However, Later on, and in the following chapters, several handy tools and simulation software will be introduced for the interpretation of EPR data. These tools are based on the simplified operator H_s. It is important to realize that a majority of the EPR spectra you will encounter in biological systems can be described accurately by this simplified operator, but not all. Therefore we will discuss the different forms of the spin Hamiltonian at the appropriate places and include the conditions under which it gives an accurate description of the EPR data and the conditions under which it will not.

1.7 Hyperfine and Superhyperfine Interaction, the Effect of Nuclear Spin

The magnetic moment of the electron can be represented as a classical bar magnet. From basic physics, we know that a bar magnet will align itself in an external magnetic field (Zeeman interaction). Physics also tells us that the energy of a bar magnet can be influenced by interaction with a neighboring bar magnet. In this latter case, the magnitude of the interaction depends on the distance of separation and the relative alignment of the two magnets.

In EPR there are three types of interaction that can occur. The first two types are due to the interaction between an unpaired electron and a magnetic nucleus. Interaction of unpaired electron with nuclear magnetic moment is termed **nuclear hyperfine interaction**. Usually called **hyperfine** if it results from the nucleus where the unpaired electron originates (Fig. 11A) and **superhyperfine** if it is from a neighboring nucleus (Fig. 11B). The third type is the interaction between two unpaired electrons on different atoms normally within a molecule, which is termed **spin-spin interaction** (Fig. 11C). Table 1.2, list the nuclei that are important in biology. Indicated are which isotopes are present (natural abundance), which of these have a nuclear spin, and the respective spin.
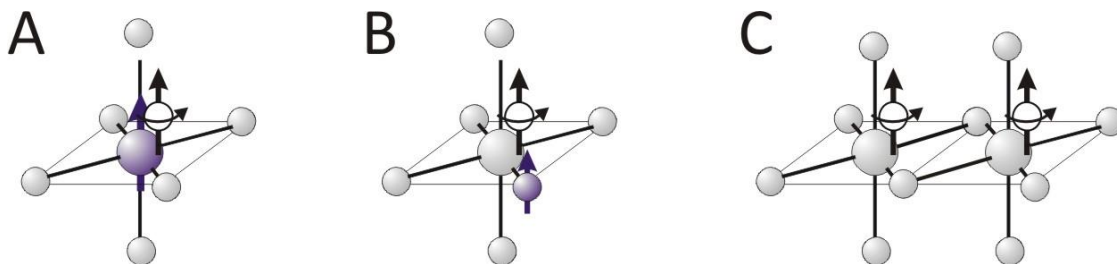

Fig. 11: Three types of magnetic interaction that can occur in EPR: Hyperfine interaction (A), superhyperfine interaction (B), and spin-spin interaction (C).

Here we will first consider systems with an electron spin and a nuclear spin. The first thing we assume is that the Zeeman interaction is much larger (two orders of magnitude or more) than the hyperfine interaction and it can be treated as a **perturbation** of the larger Zeeman interaction.

$$H_s = \beta B \bullet g \bullet S + S \bullet A \bullet I \qquad (21)$$

Where A is the anisotropic hyperfine tensor. Just like the Zeeman interaction, the hyperfine interaction will be anisotropic and it is underlined assumed that g and A are collinear.

The resonance condition becomes

$$h\nu = g\beta B_0 + hAm_I \qquad (22)$$

where A is called the **Hyperfine Coupling Constant** (Note that A is in magnetic-field units of gauss, while sometimes A' is used, which is an energy in units of cm^{-1}) and m_I is the magnetic quantum number for the nucleus. Since there are $2I + 1$ possible values of m_I ($m_I = I, I-1, ..., 0, ..., -I+1, -I$), the hyperfine interaction terms splits the Zeeman transition into $2I + 1$ lines of equal intensity. For

example, interaction of the electron with a nucleus with $I = ½$ (for example a proton) will yield an EPR spectrum containing two lines (Figs. 12 and 13). The local field of the nucleus either adds or subtracts from the applied B_0 field. As a result the ground-state and excited-state energy levels are split in two (Fig. 12). In the EPR experiment we detect now two lines instead of one (Fig. 13). Not all transitions are allowed because of selection rules.
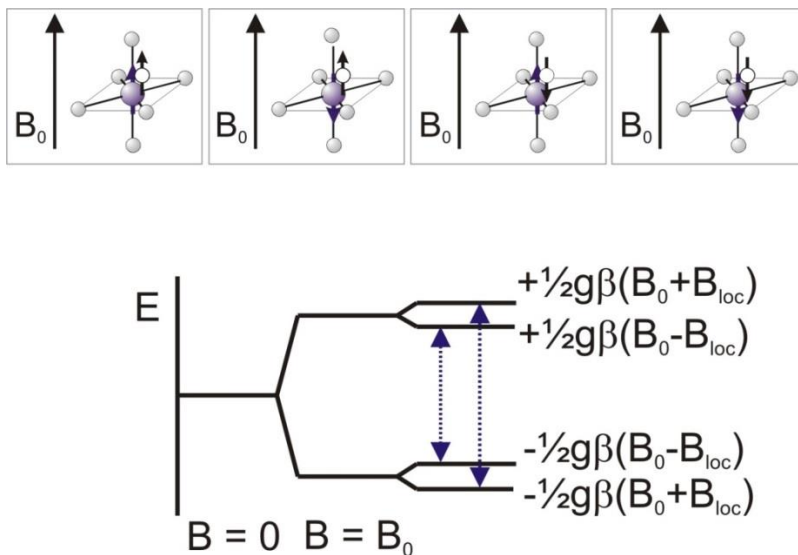

$+½g\beta(B_0+B_{loc})$
$+½g\beta(B_0-B_{loc})$

$-½g\beta(B_0-B_{loc})$
$-½g\beta(B_0+B_{loc})$

$B = 0 \quad B = B_0$

Fig. 12: Permanent local fields arising from the magnetic moments of magnetic nuclei

B_0

ΔE

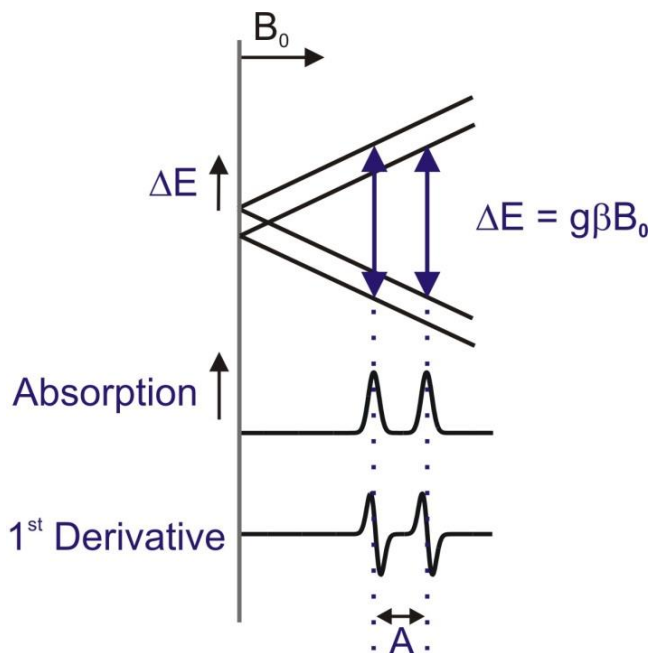$\Delta E = g\beta B_0$

Absorption

1st Derivative

A

Fig. 13: EPR experiment for a single electron interacting with a magnetic nucleus with nuclear spin $I = ½$.

Table 1.2: Nuclear spin of some nuclei that are important in biology. The isotope with a nuclear spin are indicated in blue and italics. The amount of spin and the relative abundance are indicated in the third column.

Atom	Isotope	Spin (abundance)
H	*1, 2*	^{1}H, $1/2$ (99.985); ^{2}H, 1 (0.015)
C	12, *13*	$1/2$ (1.07)
N	*14*, *15*	^{14}N, 1 (99.632); ^{15}N, $1/2$ (0.368)
O	16, *17*, 18	$5/2$ (0.038)
F	*19*	$1/2$
P	*31*	$1/2$
S	32, *33*, 34	$3/2$ (0.76)
Cl	*35*, *37*	^{35}Cl, $3/2$ (75.78); ^{37}Cl, $3/2$ (24.22)
As	*75*	$3/2$
Se	76, *77*, 78, 80, 82	$1/2$ (7.63)
Br	*79*, *81*	^{79}Br, $3/2$ (50.69); ^{81}Br, $3/2$ (49.31)
I	*127*	$5/2$
V	*50*, *51*	^{50}V, 6 (0.25); ^{51}V, $7/2$ (99.75)
Mn	*55*	$5/2$
Fe	54, 56, *57*, 58	$1/2$ (2.119)
Co	*59*	$7/2$
Ni	58, 60, *61*, 62	$3/2$ (1.14)
Cu	*63*, *65*	^{63}Cu, $3/2$ (69.17); ^{65}Cu, $3/2$ (30.83)
Mo	92, 94, *95*, 96, *97*, 98, 100	^{95}Mo, $5/2$ (15.92); ^{97}Mo, $5/2$ (9.55)
W	180, 182, *183*, 184, 186	$1/2$ (14.3)

The hyperfine interaction can make an EPR spectrum look very complex. Fig. 14 gives examples of how interactions can influence spectra, using an isotropic EPR signal.
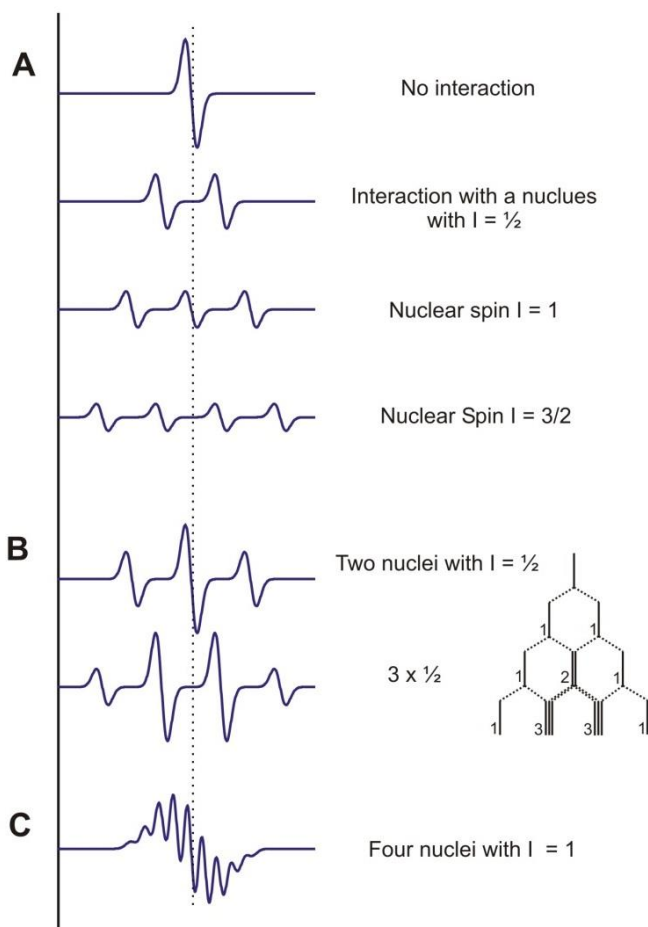

Fig. 14: Different examples of hyperfine interaction.

Fig. 14, part A, shows the interaction of the unpaired electron with different magnetic nuclei. The original signal is split in two or more signals with equal intensity. Note that the total intensity of the signal does not change and therefore the signal amplitude becomes less and less. Fig. 14, part B, shows how the line shape is affected by interaction with more than one magnetic nucleus (No correction for loss of intensity). The little 'tree' or stick diagram on the right side shows how you can calculate the relative intensities of the different bands. Fig. 14, part C, shows how a spectrum looks of a species that has interaction with four nuclei with I = 1. In the examples used in parts B and C the interactions are with nuclei that are identical. The patterns will become much more complex and at first sight much less informative when the electron is interaction with nuclei with different nuclear spins and coupling constants. Note that regardless of the number of hyperfine lines the EPR spectrum is always centered about the Zeeman transition (dotted line in Fig. 14). In other words, g can be determined from the value of the magnetic field at the middle of the spectrum (dotted line). Note, however, that in the case of half-integer nuclear spins there will not be an actual peak on this position.

With anisotropic spectra the interpretation of the powder spectrum becomes more difficult. The hyperfine splitting pattern will be the same for each of the principle g-factors but due to the anisotropy of A this is not the case for the magnitude of the splitting, which can differ significantly. Below follow a couple of example spectra to show this.

Cu^{2+} in $Cu(ClO_4)$

Cu^{2+} typically yields an axial EPR spectrum. The two principal isotopes of copper, ^{63}Cu and ^{65}Cu, both have nuclear spins of 3/2 so that the Zeeman line will be split into four lines (m_I = 3/2, 1/2, -1/2, -3/2). Since the magnetic moments of these two isotopes are very similar, the hyperfine couplings are nearly coincident. The direct consequence of the anisotropy in the central hyperfine splitting is that it is frequently much better resolved in one direction that is along a particular molecular axis than along the other two directions. The hyperfine coupling along $g_\parallel$ for Cu^{2+} is always much greater than that along $g_\perp$, resulting in a large splitting of the $g_\parallel$-line with only minor (often unobservable) splitting of $g_\perp$. An example of a powder spectrum of Cu^{2+} (d^9) is shown in Fig. 15.
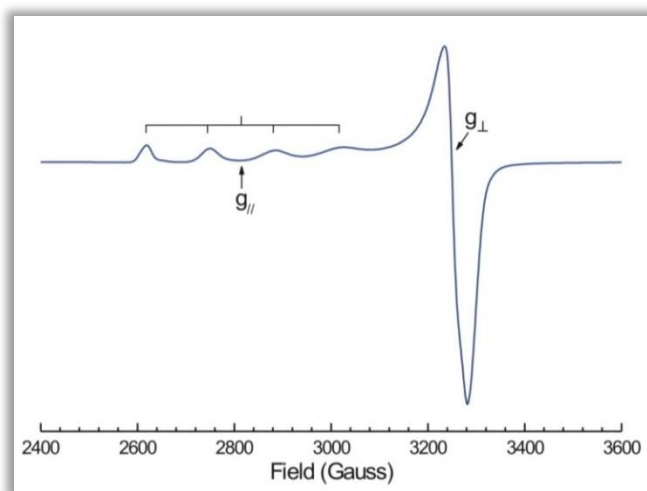

Fig. 15: EPR spectrum of $Cu(ClO_4)_2$

Ni^{1+} in methyl-coenzyme-M reductase

In methyl-coenzyme M reductase, four nitrogen atoms from the tetrapyrrole F_{430} coordinate the nickel (Fig. 16). Now we have a case of superhyperfine interaction. The paramagnetic Ni^{1+} (d^9) is coordinated by four nitrogen atoms of which the nuclei have a nuclear spin 1. Fig. 16 shows two spectra. The top spectrum shows the spectra obtained of methyl-coenzyme M in the so-called red1 state. The superhyperfine lines due to the four nitrogen ligands can clearly be detected on the $g_\perp$-peak. The resolution of the hyperfine structure on the $g_\parallel$-peak is less but still detectable. In an effort to prove that the signals that were detected in this enzyme were due to nickel, the enzyme was enriched in ^{61}Ni, which has a nuclear spin 3/2. The bottom spectrum in Fig. 16 shows the resulting spectrum. In addition to the superhyperfine structure from nitrogen we also detect hyperfine structure due to the nickel isotope. The $g_\parallel$-peak is now split into four lines. The splitting on the $g_\perp$-peak is only detectable as a line broadening since the hyperfine splitting is less than the line width of the peak. Note that this spectrum is very similar to that of Cu^{2+} in Fig. 15. In both cases we have d^9 systems.
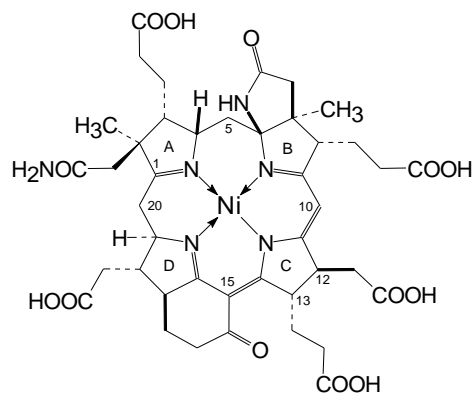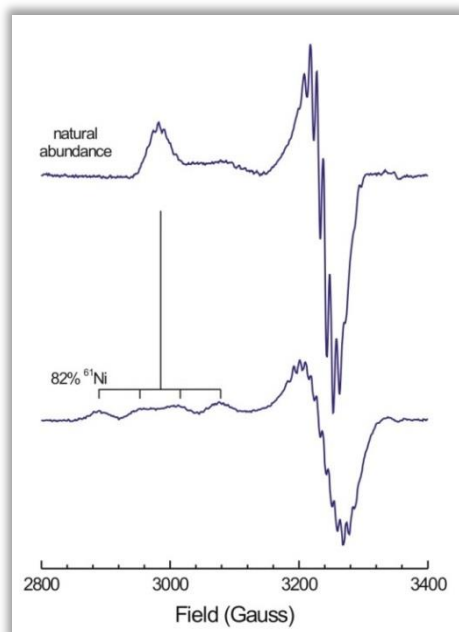
Fig. 16: EPR spectra of methyl-coenzyme M from *Methanothemobacter marburgensis* in the red1 state. The top spectrum shows the spectrum obtained after growing cells with natural abundance nickel isotopes. The bottom spectrum shows the spectrum obtained after growing cells on ^{61}Ni (I = 3/2). The structure of cofactor 430 (F$_{430}$) is shown on the right.

V^{4+} in chloroperoxidase

In the reduced form of the enzyme, the spectrum of V^{4+} (d^1) can be observed (Fig. 17). Because vanadium has axial symmetry, its powder spectrum consists of two major peaks ($g_\perp$ = 1.95 and $g_{//}$ = 1.98). Vanadium possesses one stable isotope ^{51}V with I = 7/2. Therefore each peak will be further split into eight (2I + 1) lines. Due to overlap, not all lines are observed. On top of that the Hyperfine Coupling Constant A is very large, causing the hyperfine lines of $g_\perp$ to pass the $g_{//}$-peak, causing an effect termed **overshoot**. The lines of the $g_\perp$-peak will have a different orientation when they are present on the site of the $g_{//}$-peak opposite to that of the position of the $g_\perp$-peak. The same is true for the hyperfine lines of the $g_{//}$-peak.
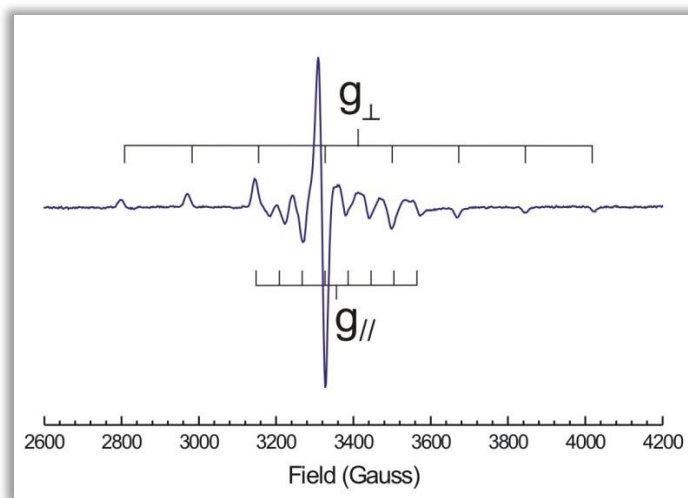

Fig. 17: Vanadium-containing chloroperoxidase from the fungus *Curvularia inaqualis*.

Second-Order and Low-Symmetry Effects

The assumption that the nuclear hyperfine interaction is only a perturbation of the Zeeman interaction is generally true in biochemical systems measured at X-band frequency. For some transition ions, however, the central hyperfine splittings are too large to be called perturbations. The typical effect, also called second-order effect, is an unequal splitting between the hyperfine lines. In this case a second-order correction is needed to be able to get a good description of the EPR data. These types of effects are typically observed for copper spectra where A_z-values are in the range of 30-200 gauss. Note that when the two interactions become equal in magnitude none of the resonance expressions in this section will be valid and the analysis requires a numerical approach.

Another effect that is also commonly observed for copper spectra is the low-symmetry effect. In low-symmetry systems the axis system that defines the anisotropy in the *g*-value need not necessarily be the same axis system that defines the anisotropy of a central hyperfine system. Thus also referred to as **tensor noncolinearity**. As a result the EPR spectrum becomes more complex and additional asymmetric peaks can be detected in addition to the main peaks which might make one believe the sample under study is inhomogeneous. To be able to describe and/or simulate the EPR data knowledge is needed about the rotations needed to correlate the two axis systems. This means an additional set of parameters and an increase in spectral simulation time.

1.8   Spin Multiplicity and Kramers' Systems

A system with *n* unpaired electrons has a spin equal to $S = n/2$. Such a system has a spin multiplicity:

$$M_S = 2S + 1 \tag{23}$$

And this value is equal to the number of spin energy levels. All the spin levels together are called the **spin multiplet**. An essential difference between $S = \frac{1}{2}$ systems and high-spin or $S \geq 1$ systems is that the latter are subject to an extra magnetic interaction namely between the individual unpaired electrons. Unlike the electronic Zeeman interaction this interaction is always present and is independent of any external field. Another name for this interaction therefore is **zero-field interaction**. In biological transition-ion complexes this zero-field interaction is usually significantly stronger than the Zeeman interaction produced by an X-band spectrometer.

The spin Hamiltonian becomes

$$H_S = \beta B \bullet g \bullet S + S \bullet D \bullet S \tag{24}$$

In the further discussion it is important to make the distinction between **half-integer systems** or **Kramers' systems** with $S = n/2$ (3/2, 5/3, etc.), and **integer systems** or **non-Kramers' systems** with S $= n$ (1, 2, etc.). Solving the wave equations it can be shown that in zero field, the sub levels of a half-integer spin multiplet group in pairs (**Kramer pairs**) and these pairs are separated by energy spacings significantly greater than the X-band microwave energy *hv*. These spacing are also called **zero-field splittings**, or ZFS. As an example let's look at the high-spin Fe^{3+} ion which has five unpaired electrons. This type of ion can either be found coordinated by four Cys residues in rubredoxins or

within a tetrapyrrole structure forming a heme group. Figure 18 shows the energy diagram for the high-spin Fe^{3+} ion in these systems.

$|m_s = \pm 5/2\rangle$

$|m_s = \pm 3/2\rangle$

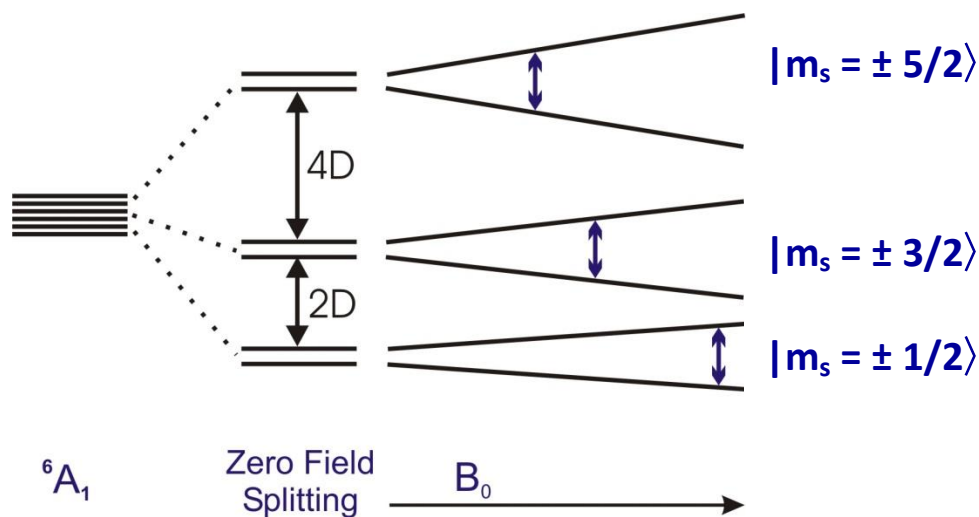$|m_s = \pm 1/2\rangle$

$^6A_1$

Zero Field Splitting

B_0

Fig. 18: Zero-field splitting effects in S = 5/2 systems with a zero field splitting parameter (D) that is large compared to the microwave frequency.

The important aspect here is that the S = 5/2 multiplet forms three Kramers' doublets that are separated from the others by energies significantly larger than the ~0.3-cm^{-1} microwave quantum (X-band). Note that the doublets are labeled with the quantum number m_s. The doublets, however, are linear combinations of the different levels but the EPR selection rule $|\Delta m_s|$ = 1 still applies.

The degeneracy between the pairs is lifted in an external field. Since the zero field splitting is very large the external field-induced splitting allows for the occurrence of EPR transitions within each (split) pair of levels. There is no crossing over and mixing of the energy levels. For Kramers' systems each Kramer's pair can give rise to its own resonance. Each of these can be described in terms of an effective S = ½ spectrum with three effective g values.

$$hv = g^{eff}\beta B \tag{25}$$

g^{eff} encompasses the real g-values plus the effect of the zero-field interaction. Just like the g-value and A-values also the zero-field interaction parameter can be anisotropic and have three values, D_x, D_y, and D_z. In contrast to g and A, however, the three D_i's are not independent because $D_x^2 + D_y^2 + D_z^2 = 0$, and so they can be reduced to two independent parameters by redefinition:

$$D = \frac{3D_z}{2} \tag{26}$$

$$E = \frac{D_x - D_y}{2} \tag{27}$$

We can also define a rhombicity

$$\eta = \frac{E}{D} \text{ with } 0 \leq \eta \leq \frac{1}{3} \tag{28}$$

From the complete energy matrix it can be derived that under the so-called weak-field limit (Zeeman interaction << zero-field interaction) the three elements of the real g tensor, g_x, g_y, and g_z, can be fixed at 2.00 and that the shape of the EPR spectra, the effective g values, is a function of the rhombicity E/D. The relationship of the effective g-values versus the rhombicity can be plotted in two-dimensional graphs, so-called **rhombograms**. The rhombogram for an $S = 5/2$ system is shown in Figure 19.
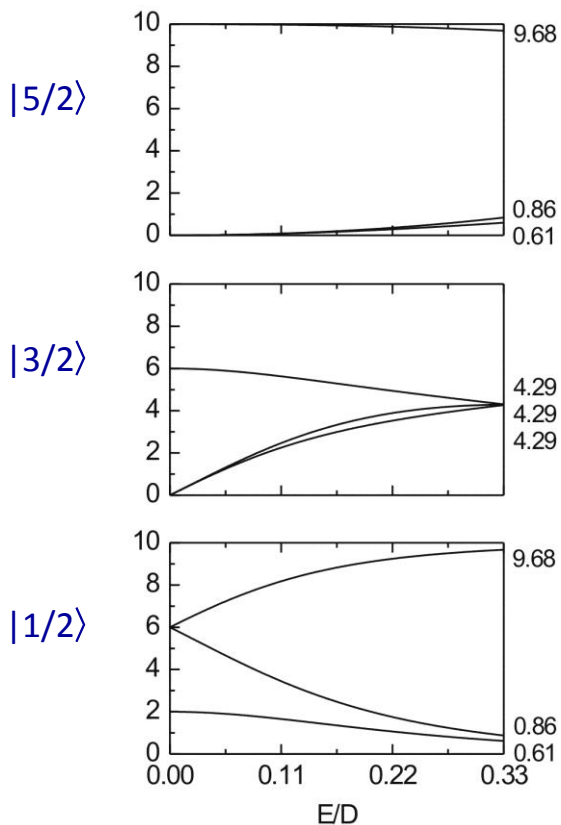

Fig. 19: Rhombogram for an S = 5/2 system.

All possible g-values for the subspectrum from a particular Kramers' doublet are represented by the three curves in the individual panels. Spectral analysis means now simply placing a ruler parallel to the vertical axes of Figure 19 and moving it along the horizontal axes to a rhombicity that produces all the experimental observed effective g-values. In practice not all g-values will be observable. Most X-band magnets go up to 1 T, precluding the detection of anything below $g = 0.6$. In addition, the highly anisotropic spectra will have very low intensity just because of the wide spread in g-values. An infinitely wide spectrum has infinitely low intensity. Visa versa the smaller the g-anisotropy, the higher the spectral intensity will be. Maximal intensity is reached when a doublet has three coinciding g-values. This is the case for the $|\pm3/2\rangle$ doublet of the $S = 5/2$ system. An $E/D = 1/3$ gives rise to the well-known $g = 4.3$ line typical for Fe^{3+} ions.

Another complication is the fact that at different temperatures different doublets will be populated and therefore spectra have to be recorded at different temperatures to fully characterize the system. In most cases more than one doublet will be occupied, even at the lowest measuring

temperature. Note that when the value of D is positive the $|\pm1/2\rangle$ doublet is the lowest lying doublet, but when the value of D is negative this doublet will have the highest energy. Below are a couple of examples to familiarize the reader with some of the high-spin signals found in biological samples.

Fe^{3+} in rubredoxin

The main feature in this spectrum (Fig. 20), measured at 4.5 K, is the very isotropic-looking peak at g = 4.32. The blow-up shows there is also a low-intense peak at g = 9.63. Taking out our ruler (red, dashed line) we can see that the spectra are due, of course, to an S = 5/2 system with E/D = 0.315, and that the 9.63 peak is due to the $|\pm1/2\rangle$ doublet (value smaller than 9.68), and the 4.32 peak is due to the $|\pm3/2\rangle$ doublet. Note that the exact value of E/D was obtained with a simulation program which will be discussed later.
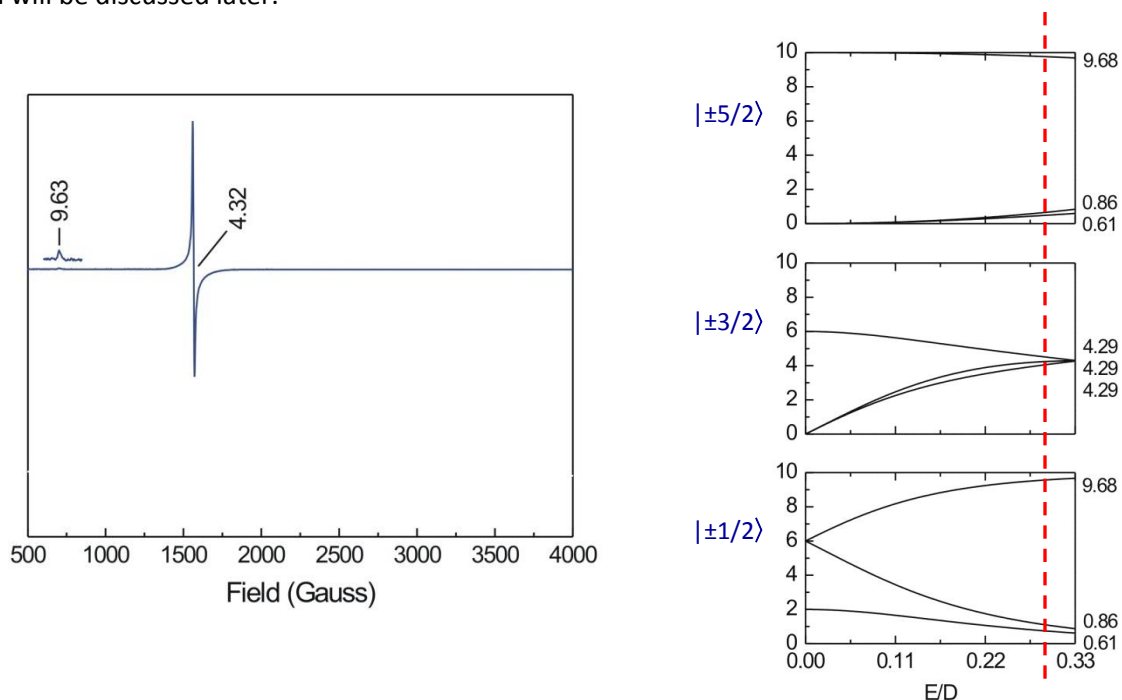

Fig. 20: EPR spectrum for Fe^{3+} in rubredoxin from *Guillardia theta* and the accompanying rhombogram indicating the effective g values for a system with E/D = 0.315

Fe^{3+}-heme in katG

In this case we get a very broad spectrum (Fig. 21) with the lowest g value at 1.99 and the highest at 6.63. This example shows a typical problem you could run into where two species are present with different rhombicity. The top two spectra in the figure are the original data (black line) and a simulation (blue line). The simulation is built up from two different species that are shown separately below this simulation. Again the signal is due to an S = 5/2 species. The first component is an axial species with E/D = 0.00 and is due to the $|\pm1/2\rangle$ doublet. The same is true for the second component, but now the spectrum is more rhombic, with E/D = 0.03. (In the actual publication the axial species was simulated with two slightly different E/D values to accommodate for the different peaks at around g = 2).
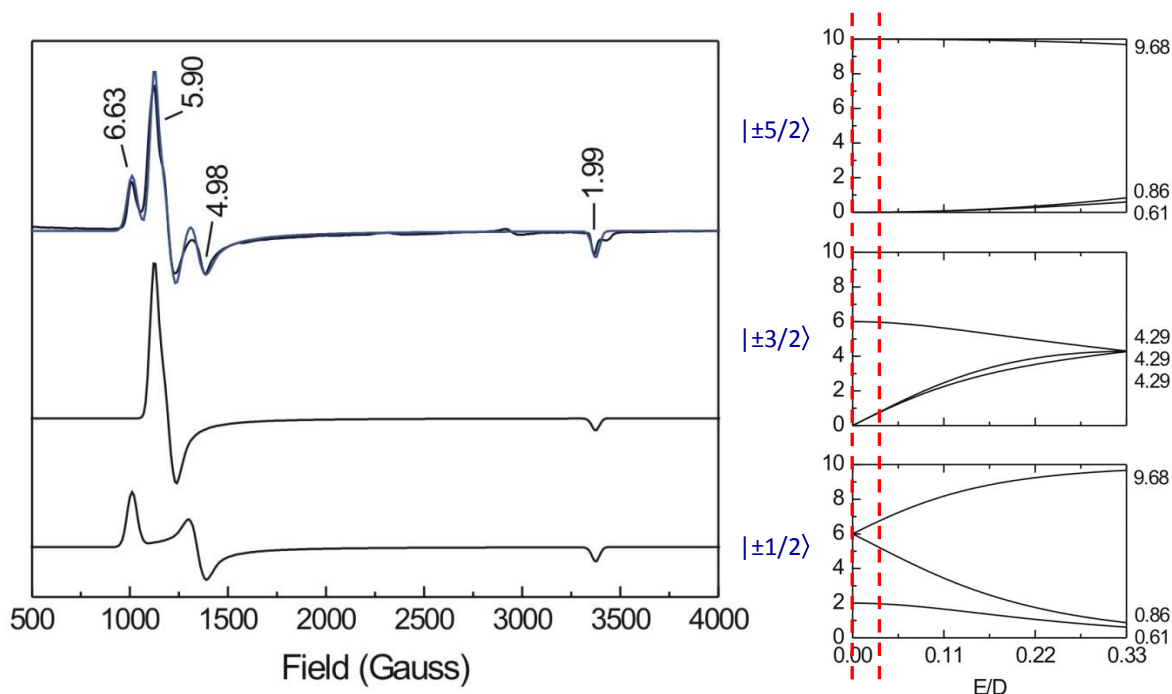
Fig. 21: EPR spectrum of Fe^{3+}-heme in katG. The top two spectra are the original data (black line) and a simulation (blue line). The two spectra below the original date are simulations of the different components with different E/D values, 0.00 and 0.03, as indicated in the accompanying rhombogram.

The rhombograms for all Kramers' systems can be found somewhere in the chapter with examples of different types of EPR signals. Note that there is always a maximal value for *g* dependent on the spin system. For *S* = ½ systems the highest *g*-value is 4. For *S* = 3/2 systems the highest *g*-value is 6, for *S* = 5/2 the highest *g*-value is 10, for S= 7/2 the highest *g*-value is 14, and for *S* = 9/2 the highest *g*-value is 18.

[2Fe-2S]⁺ in ferredoxin

The last example shows data obtained for a mutant 2Fe-ferredoxin from *Clostridium pasteurianum* (Fig. 22). This cluster has a spin *S* = 9/2. The figure shows the different spectra that can be obtained at different temperatures. The spectra are clearly different, showing that different doublets are occupied at different temperatures. The EPR spectra can be explained with an *E/D* value of 0.124 and a negative value of *D*. Note that both the |±1/2⟩ and the |±9/2⟩ doublet will have their highest g value at around 17. The order of appearance/disappearance of the other peaks, particularly the 9.59 peak and the 8.53 peaks are in line with a negative value of *D*. Also note that even at the lowest temperature there are no signals detectable due to the |±9/2⟩ doublet.
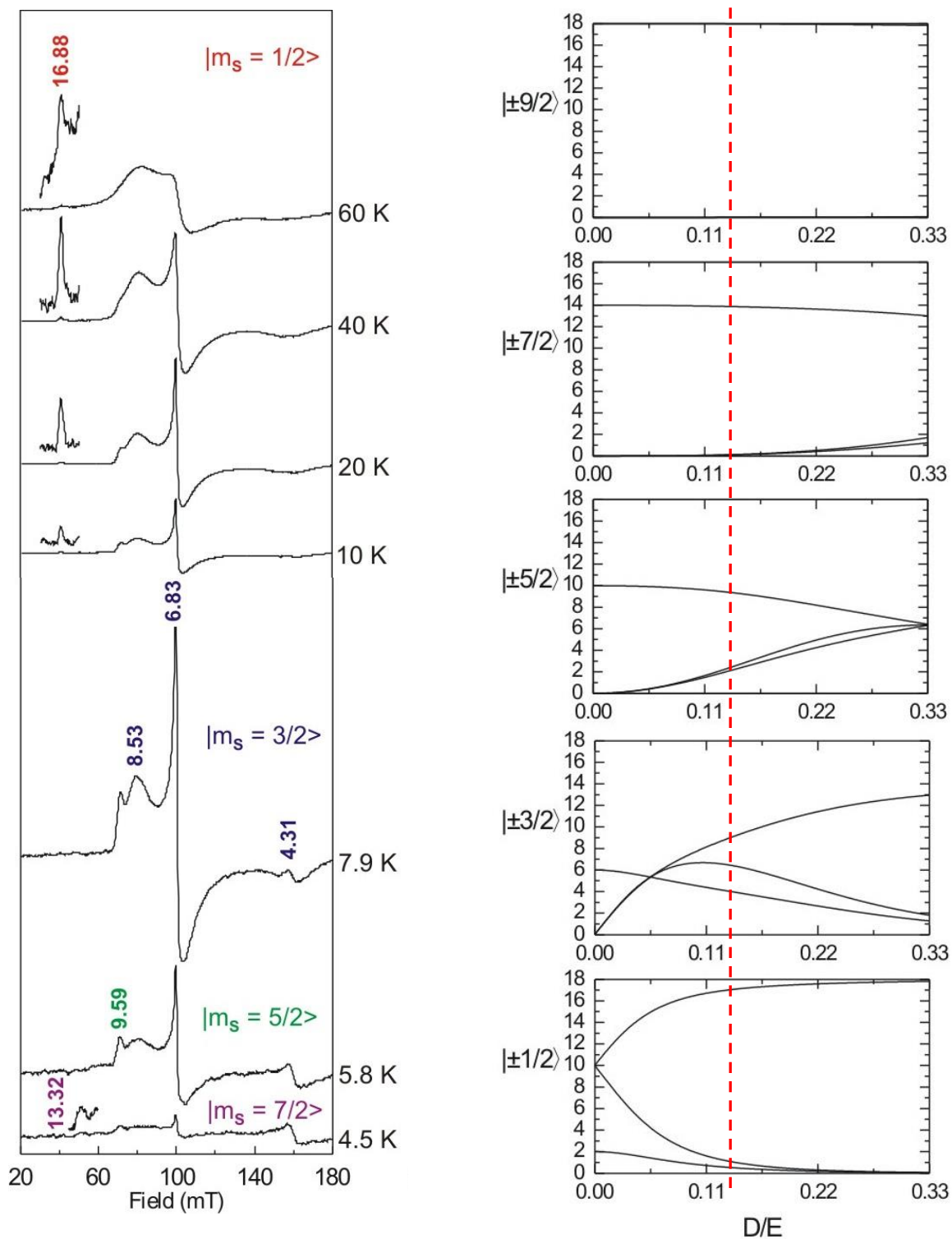
Fig. 22: EPR spectrum of the *S* = 9/2 [2Fe-2S] cluster in ferredoxin from *Clostridium pasteurianum*. The left panel shows the spectra obtained at different temperatures. The right panel shows the rhombogram for an *S* = 9/2 system. The red, dashed, line indicates the E/D value (0.124).

1.9 Non-Kramers' Systems

Non-Kramers' systems or integer systems are systems with S = 1, 2, 3, 4. These systems are very seldom observed in biological systems. One of the reasons is that just as in the Kramers' systems the energy levels are organized in doublets (and one singlet, $|0\rangle$). These doublets, however, are split even at zero fields and this splitting is generally greater than the energy of the X-band radiation. This means that in most cases the signals cannot be detected. In addition, the transitions between the doublets are forbidden because the spin has to change by more than ±1 and are very weak in the normal EPR spectrometer configurations where the static magnetic component of the microwave, B_1, is perpendicular parallel to the static magnetic field, B_0. The transitions in integer spin systems, however, are enhanced when B_1 is put parallel to B_0. This requires a special experimental setup called **parallel-mode EPR**. The Bruker ER411DM "dual mode" cavity is designed for these studies. It is called dual mode because it operates in one mode with $B_1 \perp B_0$ at about 9.8 GHz, and in another mode with $B_1 // B_0$ at ca. 9.3 GHz. The only reported cases for biological systems are from different types of iron-sulfur clusters and heme groups. The most common signal detected is the S = 2 state in [3Fe-4S]^0 clusters and Fe^{2+}-heme. Figure 23 shows the S = 2 signal detected for a [3Fe-4S]^0 cluster in the hydrogenase from *Allochromatium vinosum*. Although the transition is forbidden it can still be detected in perpendicular mode EPR. The full signal, however, is detected in the parallel-mode EPR. Due to several mechanisms the EPR signals are very broad and deformed and not much information can be obtained from the signals itself. The fact that the signals can be detected, however, can be a very important piece of evidence. The lack of a signal in parallel-mode EPR is often used to exclude the presence of [3Fe-4S]^0 clusters.

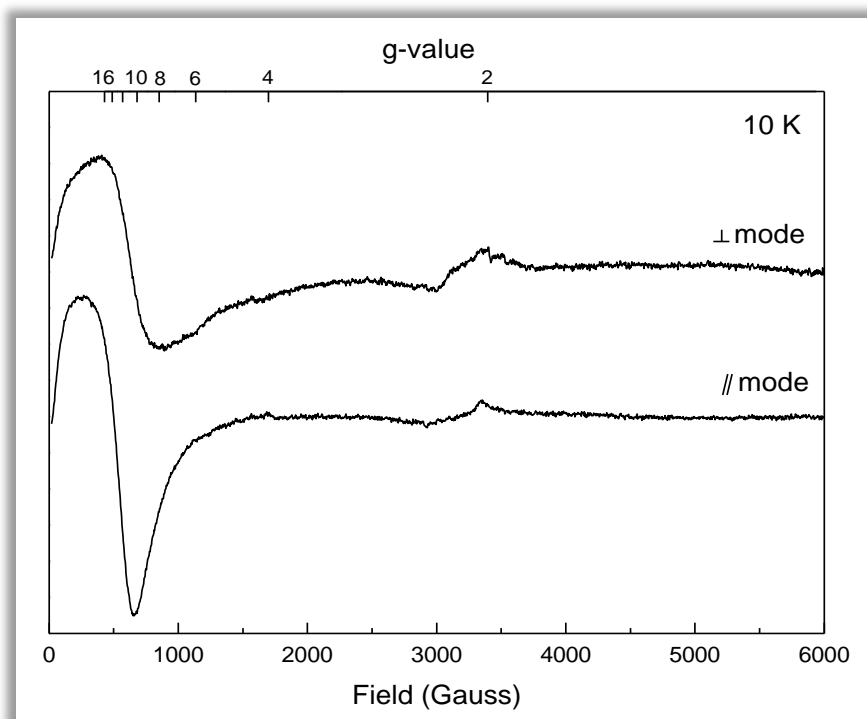**Fig. 23:** EPR spectrum of the S = 2 [3Fe-4S]^0 cluster in hydrogenase of *Allochromatium vinosum*. The top spectrum was recorded in standard EPR spectroscopy. The bottom spectrum was recorded in parallel-mode EPR spectroscopy.

1.10 Characterization of Metalloproteins

EPR spectroscopy is one of the most important techniques for the characterization of metalloproteins. There are several things that can help with identifying the metal-ion that is present. First of all only the paramagnetic forms are detectable or as we say, are **EPR active**. The properties of Fe, Ni, and Cu ions are shown in Table 1.3

Table 1.3: Electronic properties of metal ions

Metal Ion	Electron Configuration	Spin State
Fe^{2+}	d^6	S = 0 (ls) or S = 2 (hs)
Fe^{3+}	d^5	S = 5/2 (hs)
Ni^{1+}	d^9	S = ½
Ni^{2+}	d^8	S = 0 or S = 1
Ni^{3+}	d^7	S = ½
Cu^{1+}	d^{10}	S = 0
Cu^{2+}	d^9	S = ½

In the case of Fe, both redox states can potentially be EPR active, although the 2+ state normally is not. With Ni the 1+ and 3+ states are EPR active. With Cu only the 2+ state is EPR active. Therefore, in EPR studies samples are prepared of the enzyme preparation in different states: as such, reduced, and oxidized. As a reductant dithionite can be used. For an oxidant ferricyanide is commonly used. The fact that a signal can be detected in the reduced form, or the oxidized form, or both forms gives the first clue on what metal ion is present.

The next step is to look closer at the EPR signal. The position of the g-values will tell whether you are dealing with a high-spin system or not. Hyperfine splitting might be present that might give a clue about the origin of the metal ions itself. Most metals have a very unique nuclear spin. The hyperfine splitting can also indicate the presence of ligands with a nuclear spin.

From the position of the g-values we can also tell something about the type of metal ion. The spin–orbit coupling parameter is positive for S = ½ systems with less than half filled outer shells and negative for those with more than half filled shells, which means that the former have $g<g_e$ and the latter have $g>g_e$. The only exceptions to that rule are W- or Mo-containing systems.

Similar consideration can be made for more complex systems. As an example, Figure 24, shows the EPR spectra obtained for proteins containing different types of iron-sulfur clusters. There are three basic types of iron-sulfur clusters: [2Fe-2S] clusters, [3Fe-4S] clusters, and [4Fe-4S] clusters. All can be present in different oxidation states, some of which are EPR active. The 4Fe clusters come in two varieties: standard clusters that shuttle between the 1+ and 2+ oxidation states, and high-potential iron-sulfur (protein) (HiPIP) clusters that shuttle between 2+ and 3+ oxidation states.

In an oxidized protein sample that contains an Fe-S cluster you would only be able to detect a [3Fe-4S]$^{1+}$ cluster or a HiPIP [4Fe-4S]$^{3+}$ cluster. These signals are very different and easily discernable. In a reduced sample you would detect either [2Fe-2S]$^{+}$ or [4Fe-4S]$^{+}$ clusters. These signal are more

similar in shape, but as will be described later in more detail, have very different temperature behavior, with the optimal temperature for detection at around 10 K for the $[4Fe\text{-}4S]^+$ cluster and 20-70 K for the $[2Fe\text{-}2S]^+$ cluster.
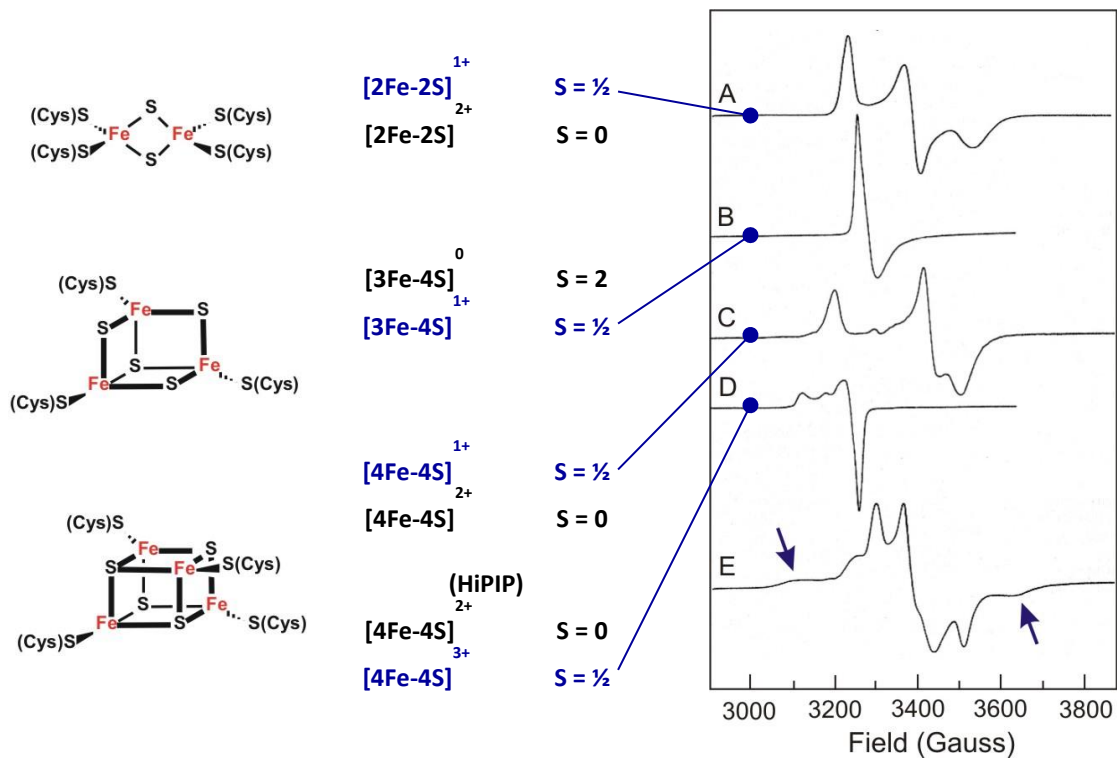

Fig. 24: EPR spectra of different types of iron-sulfur clusters. On the left the basic structure of the cluster types is shown. In the middle redox states and their respective spin states are indicated. The panel on the left show the EPR spectra of the iron-sulfur clusters in ferredoxins from *Mastigocladus laminosus* (A), *Desulfovibrio gigas* (B), *Bacillus stearothermophilus* (C), *Chromatium vinosum* high-potential iron-sulfur protein (HiPIP) (D), and *Clostridium pasteurianum* 8Fe ferredoxin (E).

1.11 Spin-Spin Interaction

In chapter 4, we will introduce the BioEPR software package for the simulation of EPR spectra. This package is very user friendly and most types of EPR spectra that will be encountered in biological systems can be simulated with this software, ranging from simple radical species to complex hyperfine spectra, high-spin systems, and some of the integer spectra. Note, however, that the software can only be used under a certain set of conditions. When these conditions are not met, different or more advanced software is needed for spectral simulation. An important example of this is found in enzymes where 2 radical species are present in close proximity of each other. In Figure 24, trace E, a spectrum is shown that is detected in a so-called 8Fe ferredoxin. In this protein two $[4Fe-4S]^+$ clusters are present. For comparison, look at trace C in Figure 24 that shows the spectrum of a single $[4Fe-4S]^+$ cluster detected in another ferredoxin enzyme. If the two clusters would be far apart and not able to sense each other, the spectrum for the 8Fe Ferredoxin would be a simple summation of two single $[4Fe-4S]^+$ spectra. If you are lucky, both paramagnets could display somewhat different g-values and it should be possible to discern both signals in the spectrum. If the distance between the two paramagnets is 10-12 Å or less, however, the two paramagnets will interact with each other and both signals would split up similar to the effect seen with hyperfine interaction. However, this is not what is detectable in Figure 24, trace E. Broad wings are detectable in the EPR spectrum (indicated by the arrows). These are generally the first indication that there are two species that are spin coupled. Note how these wings reach far beyond the region where the g-values of both paramagnets would be in the absence of the spin-spin interaction. Unlike in hyperfine interaction where the g-tensor of the electron spin and the anisotropic hyperfine tensor A are assumed to be collinear, the individual g-tensors of the two interacting paramagnets in spin-spin interaction can have every possible orientation causing the resulting EPR signal to be very different in shape. Therefore in spin-spin interaction both the distance and the angle of the respective g-tensors of the paramagnetic species are of importance.

To further complicate the interpretation of these types of signals there will also be different types of interactions dependent on the distance between the two interacting paramagnets. The two magnetic interactions that operate between paramagnetic centers are the through-space dipole-dipole interaction and an exchange interaction that depends on orbital overlap and spin polarization effects. The former is an anisotropic interaction that follows a $1/r^3$ dependence on the spacing between the interacting centers. The latter is usually considered an isotropic interaction, which falls off approximately exponentially with the distance between the partners. At distances greater than approximately 9 Å, the exchange interaction creates a doublet splitting in the EPR spectrum of each partner. At closer distances, the exchange interaction mixes the two spin systems, such that their g-values become averaged and eventually converge to a triplet state at interspin separations of <7 Å.

To understand the shape of the interaction spectra, a second example is discussed here and is from a family of enzymes called adenosylcobalamin (coenzyme B_{12})-dependent isomerases. These enzymes catalyze skeletal rearrangements via a radical mechanism. The reaction starts with the generation of the 5'-deoxyadenosyl radical and cob(II)alamin from enzyme-bound adenosylcobalamin by homolysis of the coenzyme's cobalt-carbon σ-bond in the presence of a substrate molecule SH. Stereospecific hydrogen abstraction from the substrate molecule by the 5'-deoxyadenosyl radical gives 5'-deoxyadenosine and a substrate radical S$^\bullet$. At this point two paramagnetic species are present in the enzyme, the Co^{2+} species and the S$^\bullet$ radical species (Fig. 25).
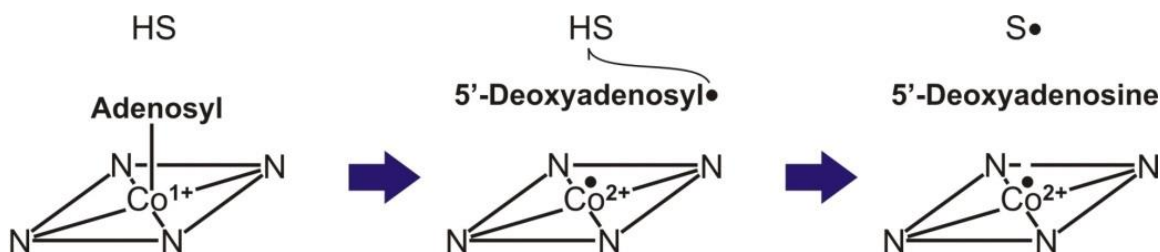
Fig. 25: Formation of the two paramagnetic species in adenosylcobalamin (coenzyme B$_{12}$)-dependent isomerases.

To be able to understand the reaction mechanisms of these enzymes in detail, it is important to determine what radial species are present at different reaction times and where they are located in the enzyme active site. The distance between the Co^{2+} and the deoxyadenosyl or the substrate-based radicals can be obtained from simulation of the detected EPR spectra. For distances larger than 4-5 Å both paramagnets can be considered point dipoles. The dipole–dipole interaction lifts the degeneracy of the spin states in the absence of an external magnetic field and is a source of zero-field splitting. In the most general formulation, the zero-field splitting is described as a traceless tensor with an axial, D, and a rhombic, E, term. In the commonly used point-dipole approximation, E ≡ 0. The principal axis of the zero-field splitting normally contains the interspin vector. In simulations, Euler rotations (θ) are required to relate the axis system of the zero-field splitting tensor to a reference system, such as the g-axis of Co^{2+} (Fig. 26). The EPR spectra are normally interpreted with the aid of a spin Hamiltonian containing the g- and A-tensors of the individual radicals, as well as the exchange and dipole–dipole interaction terms of the spin–spin coupling. Good approximations for the g- and A-tensors of cob(II)alamin bound to the enzyme of interest are frequently available, such that the spin-spin interaction terms and Euler angles relating the interspin vector to an appropriate molecule fixed axis (e.g. the g-axis of Co^{2+}) are the major unknowns in the analysis.
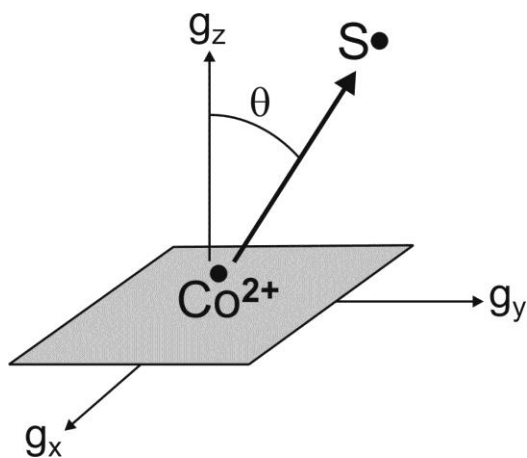

Fig. 26: Position of the substrate radical in respect to the position of the Co^{2+}
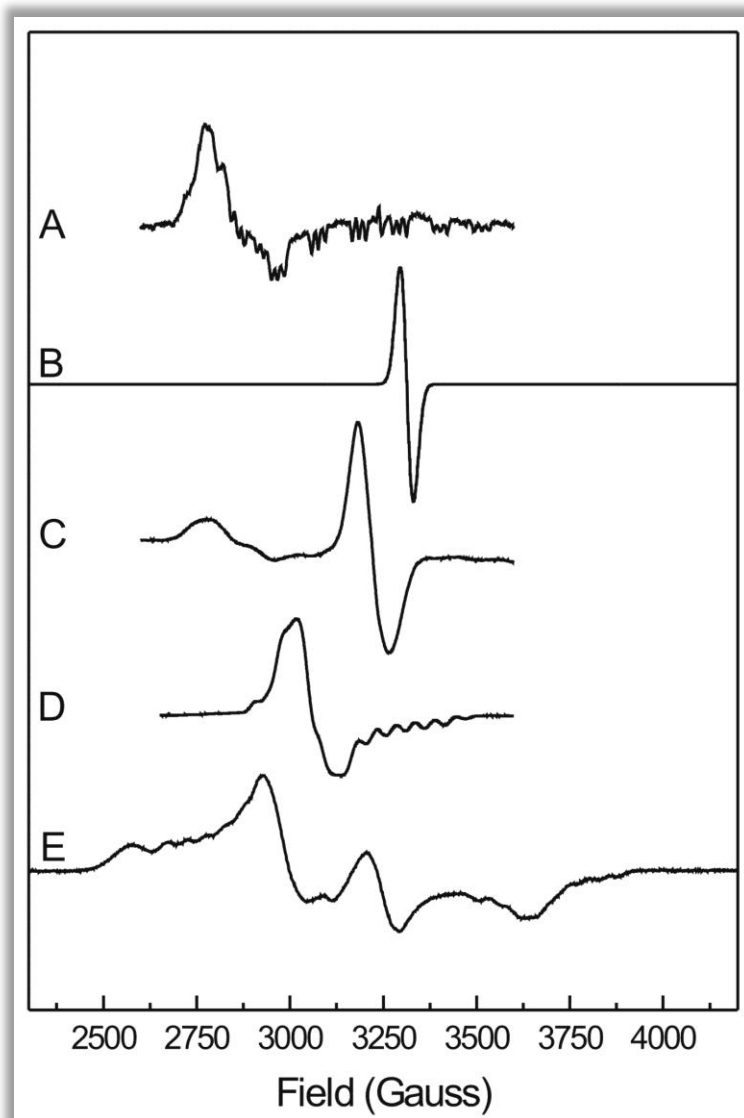
Fig. 27: (A) Co^{2+} signal detected in ethanolamine ammonia lyase obtained by reacting the enzyme with a suicide inactivator (e.g. methanol) that escapes from the active site after forming the substrate radical and becomes quenched. This leaves behind the isolated Co^{2+} signal. (B) Simulation of a radical species with g = 2.0023. (C) Signal of the coupled Co^{2+}/radical species in ethanolamine ammonia lyase after reacting with ethanolamine. The interspin distance is 8.7 Å and θ = 25° (D) Coupled Co^{2+}/radical species in lysine-5,6-aminomutase after reacting with 4-thialysine. The interspin distance is 7.0 Å and θ = 43°. (E) Coupled Co^{2+}/radical species in diol dehydratase after reacting with 5'-deoxy-3',4'-anhydroadenosylcobalamin. The interspin distance is 3.5 Å and θ = 75°.

Figure 27, shows a set of spectra from different adenosylcobalamin-dependent isomerases. The first spectrum (Fig. 27, trace A) is the Co^{2+} spectrum observed in ethanolamine lysase after quenchiong of the radical species. This is an example of the Co^{2+} spectrum when there is no interaction with a second paramagnet. The spectrum is axial, with the $g_{/\!/}$ peak on the high-field site. The whole spectrum is split in 8 lines due to the nuclear spin of the cobalt ion (I = 7/2). On top of that there is interaction of the electron in the d_{z^2} orbital with an axial nitrogen ligand which causes and additional

3-fold split of each of the 8 lines. Note that the hyperfine splitting of the $g_\perp$ peak is not resolved. The $g_\parallel$ peak, however, shows a large hyperfine coupling. Of the expected 8 lines, 6 can be easily recognized, including the additional 3-fold split. Two of the lines overlap with the $g_\perp$ peak and are more difficult to discern. In the chapter with examples of different types of spectra a Co spectrum is shown recorded at higher frequency. In this case the lines of the $g_\parallel$ peak do not overlap with the $g_\perp$ peak and the 8 lines can be easily recognized. (The effect of different frequencies on EPR signals will be discussed in section 1.12). Also shown in Figure 27, trace B, is a simulation of a radical species.

Weakly coupled spin systems

Shown in a separate figure (Fig. 28) is an example of a weakly coupled system. The suicide inactivation of ethanolamine ammonia-lyase by hydroxyethylhydrazine results in the formation of a hydrazine cation radical that is positioned 13 Å from Co^{2+} and approximately along the $g_\parallel$-axis of the ion (i.e. directly above the plane of the corrin ring). The individual radical species can easily be recognized in the measured EPR spectrum (Fig. 28). The signals from the low-spin Co^{2+} and the partner radical were split by a combination of exchange and dipole-dipole coupling. This can be detected as the additional hyperfine splitting of the Co^{2+} signal (Compare with Figure 27, trace A).
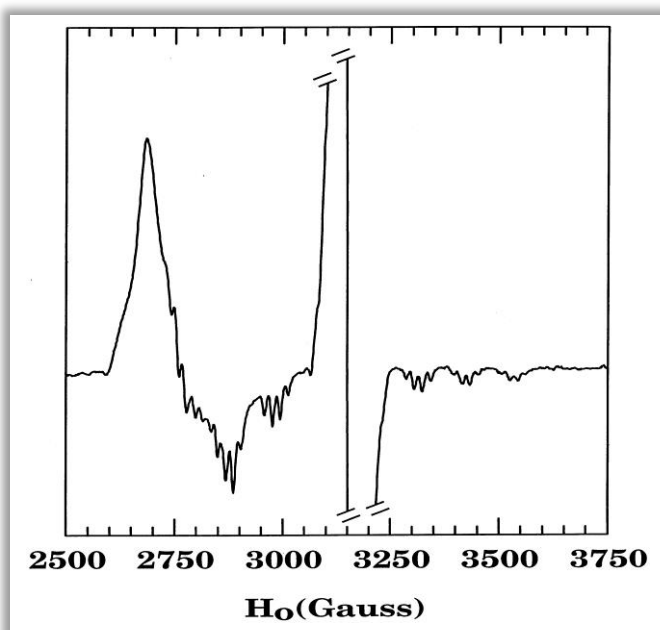

Fig. 28: X-Band EPR spectrum of hydroxyethylhydrazine-inactivated ethanolamine ammonia-lyase showing presence of features corresponding to B_{12r} and a companion radical species with absorption near g = 2.0. The amplitude of the signal of the radical centered at g = 2.0 is off scale. (Taken from Bandarian, V., Reed, G.H., Biochemistry (1999) 38, 12394-12402)

Strongly coupled spin systems

In Figure 27, traces C and D are representatives of cases where there is a strong coupling between the cobalt and the radical species. In trace C the spectra of the two paramagnets have moved closer towards each other and there are clear differences in the shapes of the signals. In trace D the EPR

spectra appears to be a hybrid of both the cobalt and the radical EPR signals and exhibit an average g-value of ≈ 2.1 that arises from coupling between a carbon centered radical (g = 2.0023) with cob(II)alamin (g_{av} ≈ 2.18). The signals are due to a 'hybrid' triplet spin system comprising both paramagnetic species. Trace C in Figure 27 is detected in ethanolamine ammonia lyase after reacting with ethanolamine. The interspin distance is 8.7 Å and θ = 25°. Trace D in Figure 27 is from lysine-5,6-aminomutase after reacting with 4-thialysine. The interspin distance is 7.0 Å and θ = 43°.

Very strongly coupled spin systems

The last example spectrum in Figure 27, trace E, is a signal detected in diol dehydratase after reacting with the analog 3',4'-anhydroadenosylcobalamin (anhydro-AdoCbl). This gives a more stable allylic radical upon hemolysis of the cobalt–carbon bond, creating a somewhat stable radical very close the Co^{2+}. The EPR spectrum (Fig. 27, trace E) does not resemble that of Co^{2+} or a radical species or the other spectra shown in Figure 27. However, it is still consistent with a rhombic triplet-state species. A prominent half-field transition at around g = 4 can be detected (not shown) which is a hallmark of strongly coupled triplet spin systems. Changes in the linewidths of transitions in the EPR spectra resulting from ^{13}C and ^{2}H isotopic substitutions in the anhydroribosyl moiety identified one of the triplet spin partners as the anhydroadenosyl radical. The presence of ^{59}Co hyperfine splitting, as well as the apparent g-values of the signals, identified low-spin Co^{2+} of cob(II)alamin as the other spin in the hybrid triplet system. Note that also in this case the EPR spectrum covers an area much wider than one would expect based on the g-values of the two individual paramagnets (Fig. 27, traces A and B). The spectrum can still be simulated using the point-dipole approximation, but to get a more accurate value for the distance and the Euler a higher level of treatment is required. The spectrum can be simulated using an interspin distance of 3.5 Å and a θ of 75°.

1.12 High-Frequency EPR Spectroscopy

Why would we use different frequencies in EPR spectroscopy? Going back to Figure 5, you can see that an increase in the strength of the magnetic field B_0 will result in a larger separation of the two energy levels. As a result there will be an increased population difference between the ground and excited state resulting in higher signal amplitude. To be able to meet the resonance conditions the frequency will also have to be increased according to $g = 0.7145\,\nu/B_0$. For both technical and fundamental reasons, however, it turned out that the optimum sensitivity in EPR is reached in the 8-12 GHz range and X-band is right there in the middle of that range. This is the reason that X-band EPR spectroscopy is the most common EPR technique. There are cases, however, that the information obtained at X-band frequencies is limited and a higher frequency is needed. EPR absorption lines can have a width that is independent of the used frequency and the corresponding resonance field. As a consequence, the resolution of two partially overlapping lines will increase with increasing frequency as illustrated in Figure 29. Note that there is a theoretical limit of maximal resolution enhancement by frequency increase. In practical cases the enhancement is usually less or in some cases there is no enhancement at all.
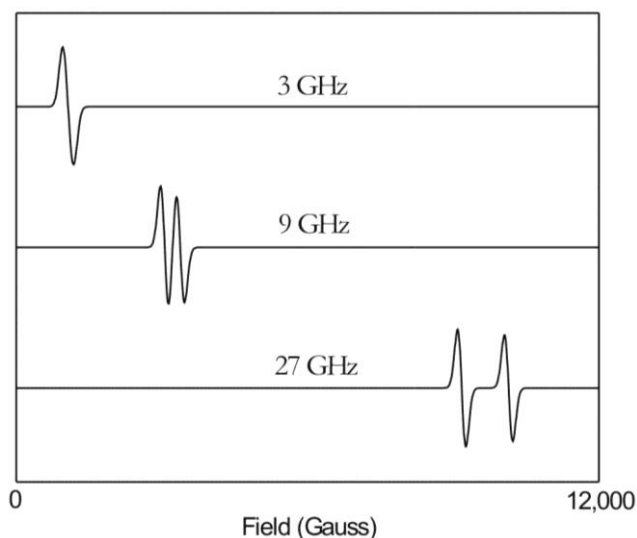

Fig. 29: Theoretical increase in resolution with increasing frequency. A two-line EPR spectrum is given at three different microwave frequencies.

Again using a practical example the extra information from using a higher frequency can be easily demonstrated. Let us go back to the Red1 signal detected in methyl-coenzyme M reductase (Figs. 16 and 30). The spectrum seems to be due to an axial species. When you count the amount of hyperfine lines on the $g_\perp$-peak, however, you will find 10 lines instead of the 9 lines you would expect for an interaction with four N nuclei (Fig. 30, top). It turns out that the signal is slightly rhombic and the g_x and g_y have two different values. The difference is such that there is still a perfect match between the hyperfine lines, but one set is just shifted so that an additional peak can be detected.

When the same species is now measured at W-band (90 GHz) the signal looks much different. First of all the hyperfine structure is lost. This is due to the fact the Hyperfine Coupling Constant A is not dependent on the frequency. The additional splitting of the energy levels is now negligible in

comparison to the splitting due to B_0, and as a result is no longer detected. The line widths of the signal did not change, but the peaks are now more spread apart. The peaks, however, can be matched by squeezing the W-band spectrum horizontally. Now to the eye it looks like the peaks have become much sharper and the g_y- and g_x-peaks are nicely resolved. Note that the best way to compare spectra at different frequencies is to use the only property that does not change, the g-value. The same plot can be obtained if both spectra are plotted using a g-scale. Note, however, that the g-scale is a reciprocal scale and not a linear scale.
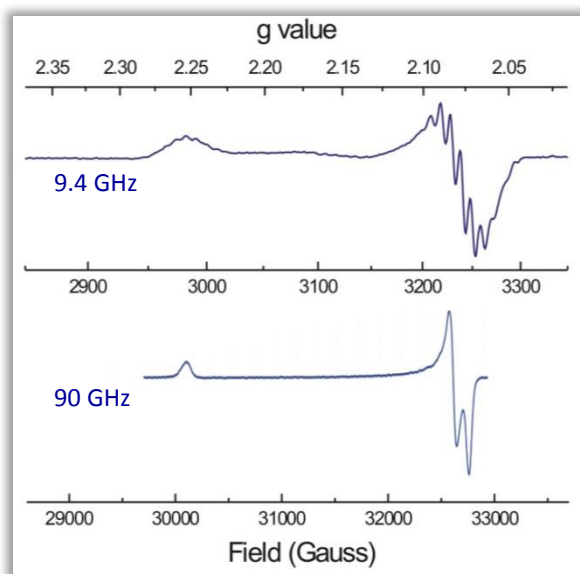

Fig. 30: EPR spectra of the Ni^{1+} signal (red1) detected in methyl-coenzyme M reductase measured at X-band (9.4 GHz) and W band (90 GHz).

1.13 *g*-Strain

We know from folding studies and from structural NMR and X-ray studies that samples of proteins come with a distribution of conformations. For EPR this means that the paramagnet in each molecule has a slightly different structural surrounding and thus a slightly different *g*-value. This structural inhomogeneity or **g-strain** is reflected in the spectroscopy in the form of an inhomogeneous line shape. This normally results in a change from a Lorentzian to Gaussian line shape. An important consequence of this *g*-value anisotropy is that the line width, W, is in general, also isotropic.

Most of the time we do not have to worry about this, but particularly in the EPR spectra of the iron-sulfur clusters *g*-strain can have a big effect on the shape of the EPR spectrum and therefore on the simulation and interpretation of the EPR data. The most noticeable difference is now that the linewidth, plotted on a *g*-scale does not change when the spectra are measured at higher frequency. This effect is shown in Figure 31 for the [4Fe-4S] cluster detected in spinach-leaf ferredoxin. The line width is very similar in the range of 35 to 3.3 GHz. At 1.1 GHz a broadening is detected due to unresolved hyperfine coupling.
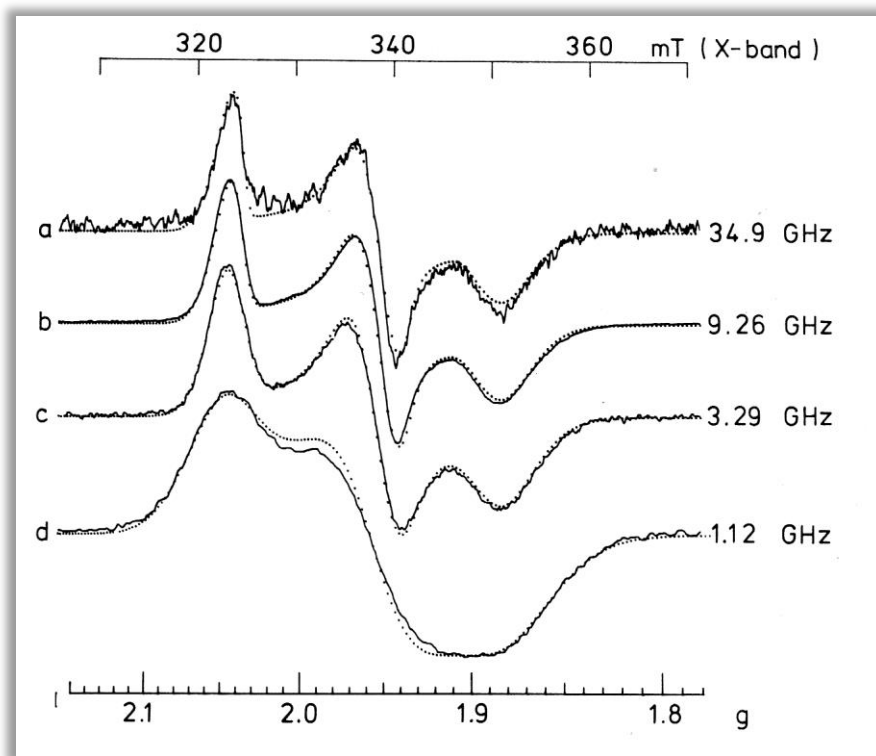

Fig. 31: Experimental and simulated spectrum of spinach-leaf ferredoxin at four microwave frequencies.

The example in Figure 30 for MCRred1-Ni(I), showed that in some cases the use of higher frequency can give additional essential information. The example in Figure 31, however, shows that this is not always the case.

1.14 ENDOR, ESEEM, and HYSCORE

In the examples we have seen up until now, the nuclear hyperfine splitting was always clearly detectable, at least in one of the peaks of the EPR signal. More often than not the hyperfine splitting is not resolved but is hidden in the EPR peaks, as in the example in Figure 31, where the spectrum contains unresolved hyperfine splitting. This interaction might be coming from a ligand or compound that is bound to the paramagnetic metal ion in the active site of an enzyme of interest. Since knowledge of this information could be important to gain more insight into the properties and function of the metal ion, techniques have been developed to detect these interactions. These are normally pulsed techniques also referred to as advanced techniques. The two main techniques are *E*lectron *S*pin *E*cho *E*nvelope *M*odulation (ESEEM) and *E*lectron-*N*uclear *DO*uble *R*esonance (ENDOR) spectroscopies. In transition metal complexes and metalloproteins, magnetic nuclei such as ^{1}H, ^{2}H, ^{13}C, ^{14}N, ^{15}N, ^{17}O, ^{31}P and ^{33}S, in the vicinity of the paramagnetic metal ion can be detected by these techniques. Not only do ENDOR and ESEEM enable one to identify the presence of a particular ligand nucleus but under favorable circumstances metal-ligand nuclei distances and angles can be obtained as well. Although both techniques give similar types of information about your enzyme, depending on the interaction parameters, the sensitivity of the two techniques can be drastically different. Sometimes only one of the techniques can be employed and there are situations where complementary results are obtained from ESEEM and Pulsed ENDOR. The sensitivity of ESEEM is highest at low hyperfine transition frequencies and decreases with increasing frequency due to the limited microwave field strength. The sensitivity of Pulsed ENDOR is approximately proportional to the hyperfine transition frequency. At zero frequency, the ENDOR sensitivity is zero. ENDOR is therefore extremely difficult at low transition frequencies whereas it has a high sensitivity for high frequencies.

Let us now consider the spin Hamiltonian relevant for these techniques. Equation 29 shows the spin Hamiltonian for the simplest system, with effective electron spin *S* = ½ and a single nucleus with *I* = ½

$$H_s = \beta_e B \bullet g_e \bullet S - \beta_n B \bullet g_n \bullet I + S \bullet A \bullet I \tag{29}$$

Where β_e and β_n are electronic and nuclear magnetons, *g* and g_n are the electronic and nuclear *g*-tensors, and *A* is the anisotropic hyperfine tensor describing the interaction between the electronic and nuclear spins. In this equation, the first term is the electronic Zeeman interaction, the second is the nuclear Zeeman interaction, and the third is the hyperfine interaction.

The energies to first order are given by the expression

$$E(m_s m_I) = g_e \beta_e B m_s - g_n \beta_n B m_I + h A m_s m_I \tag{30}$$

Figure 32 shows the energy level diagram calculated from equation 30 and illustrates the splitting of the spin states by the successively smaller interactions for a magnetic field of approximately 3300 G.
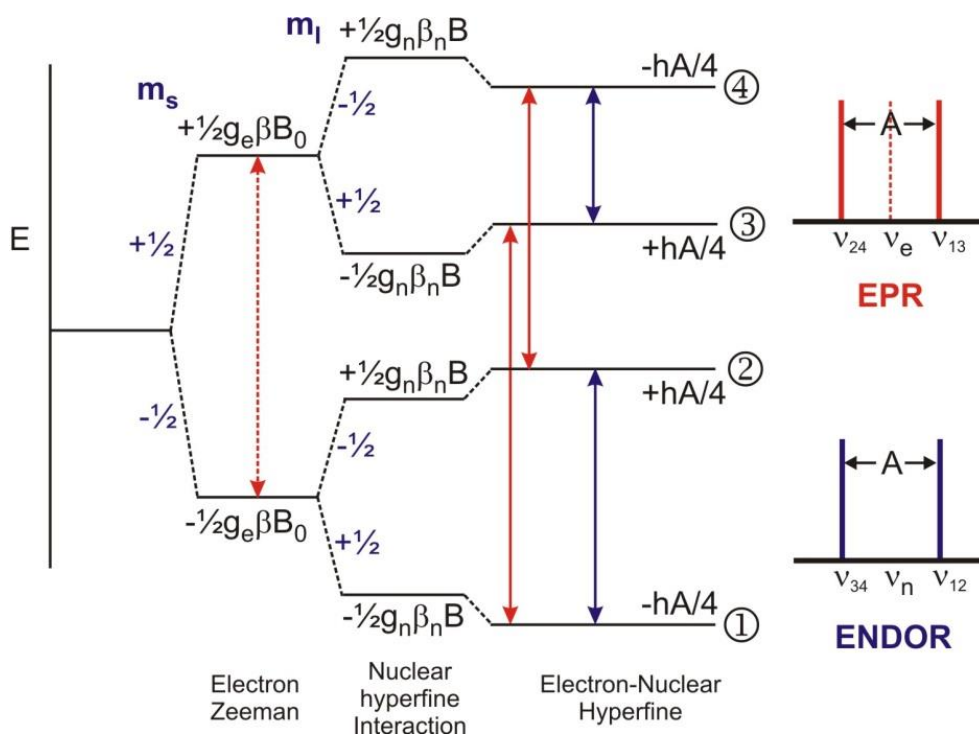
Fig. 32: Energy level diagram for an *S* = ½, *I* = ½ spin system. The *g*-value and hyperfine coupling are assumed to be isotropic. The red lines show the allowed EPR transitions and the stick EPR spectrum. The blue lines show the NMR (ENDOR) transitions and the stick ENDOR spectrum.

Two types of transitions are indicated in the figure. First are the usual EPR transitions occurring at frequencies v_{13} and v_{24} and indicated by red lines between levels 1 and 3 and between levels 2 and 4. These transitions obey the usual EPR selection rule $|\Delta m_s| = 1$, $|\Delta m_I| = 0$ where only electron spin flips but no nuclear spin flips are allowed. The second transitions, indicated by blue lines, are NMR transitions ($|\Delta m_s| = 0$, $|\Delta m_I| = 1$) and occur at the frequencies v_{12} and v_{34}. These frequencies are also known as the ENDOR or ESEEM frequencies. The little stick spectra on the right hand side/top show what the EPR spectrum would look like if the lines were resolved (v_e is the position of the original, unsplit, EPR peak). The bottom stick spectrum shows what the ENDOR spectrum will look like. The splitting by the coupling constant *A* is indicated.

The ENDOR spectrometer essentially consists of a standard CW EPR spectrometer with an NMR radio frequency (rf) source and an rf coil within the microwave cavity. This arrangement enables EPR and NMR experiments to be performed simultaneously on the sample. In CW ENDOR, the EPR signal at a given field is partially saturated by an increase of microwave power. When the radio frequency matches a nuclear frequency, in another word, when a nuclear transition is induced, the population of the partially saturated EPR transition will be changed and the recovery of this signal will be realized by detecting net microwave absorption. The resonance lines are inherently narrower in ENDOR than in EPR spectroscopy and the chief use of ENDOR in the metalloprotein investigations is that it enables weaker hyperfine interactions to be resolved. In addition, nuclei can be unambiguously identified by their ***Larmor frequency***. The principle disadvantage of this technique is the greatly reduced sensitivity compared with EPR. This means that samples need to be more than 10 fold concentrated to yield acceptable ENDOR spectra.

Figure 34 shows the data obtained for a paramagnetic species detected in the enzyme (*E*)-4-hydroxy-3-methylbut-2-enyl diphosphate synthase (IspG). IspG converts 2-*C*-methyl-D-erythritol-2,4-cyclodiphosphate (MEcPP) into (*E*)-4-hydroxy-3-methyl-but-2-enyl diphosphate (HMBPP) in the penultimate step of the MEP pathway for isoprene biosynthesis. MEcPP is a cyclic compound and the reaction involves the opening of the ring and removal of the C3 hydroxyl group consuming the total of two electrons.
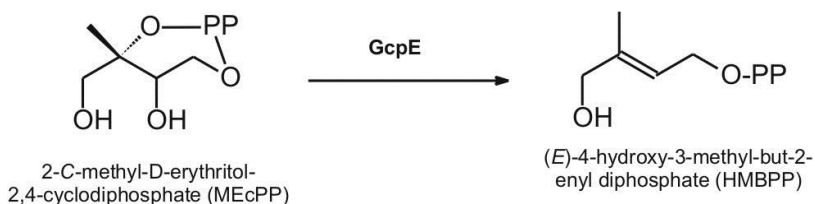

2-*C*-methyl-D-erythritol-
2,4-cyclodiphosphate (MEcPP)

(*E*)-4-hydroxy-3-methyl-but-2-
enyl diphosphate (HMBPP)

Fig. 33: Reaction catalyzed by GcpE

The enzyme contains a single [4Fe-4S] cluster in its active site. In kinetic studies where the enzyme was incubated with dithionite and the substrate MEcPP a paramagnetic species was detected that displayed a rhombic EPR signal with g_{xyz} = 2.000, 2.019, and 2.087 (Fig. 34, panel A. See also the freeze-quench section in chapter 2). The spread in *g*-values would argue against a radical-type species. In addition, labeling with [57]Fe caused extensive broadening of the EPR signal, indicating it is Fe-based and most likely represents and new form of the Fe-S cluster. Note that this species does not have any resemblance with the standard type iron-sulfur cluster signals shown in Figure 24. It was proposed that the substrate MEcPP binds to the cluster during the reaction mechanism, most likely via the –OH group that is removed in the reaction (Fig. 34, panel B). Figure 34, panel C, shows the ^{31}P-ENDOR measurements for this signal. At six different field positions an ENDOR spectrum was obtained. These are indicated on the absorption EPR signal (Under the saturation conditions used in ENDOR not the first derivative, but the 'regular' absorption-type signal is measured.) Note that the ENDOR was obtained at Q-band frequency (35 GHz) and therefore the field values do not match with those of panel A. The *g*-values are included for easy comparison. The EPR species showed a weak ^{31}P coupling which was detectable over the whole EPR envelope. From the coupling constant a distance of 5-6 Å could be estimated which is in line with binding of the substrate to the enzyme in close proximity of the active-site cluster. In a separate experiment (see below) using [17]O labeled MEcPP, a very short distance between the cluster and the [17]O atom was found.

*E*lectron *S*pin *E*cho *E*nvelope *M*odulation (ESEEM) is an important technique for measuring the hyperfine interaction parameters between electron spins and nearby nuclear spins. From the analysis of the ESEEM signals detailed information about electron spin density distribution, distances and bonding angles is gained. An extension of this technique is *HY*perfine *S*ub-level *COR*r*E*lation (2D-HYSCORE). This technique is essentially a two dimensional ESEEM experiment in which correlation is transferred from one electron spin manifold to another. HYSCORE allows one to take a complicated ESEEM spectrum and extend the data into a second dimension. Peaks appearing in the upper right and lower left quadrants of the 2D spectra typically arise from nuclei in which the hyperfine coupling is less than the Larmor frequency. They appear at the Larmor frequency, separated by the hyperfine coupling. Peaks from nuclei in which the hyperfine interaction is greater than the Larmor frequency appear in the upper left and lower right quadrants of the spectra. Even with the complexity of the spectra, HYSCORE on systems with multiple nuclei can make ESEEM spectra that would be difficult or impossible to interpret much more manageable.
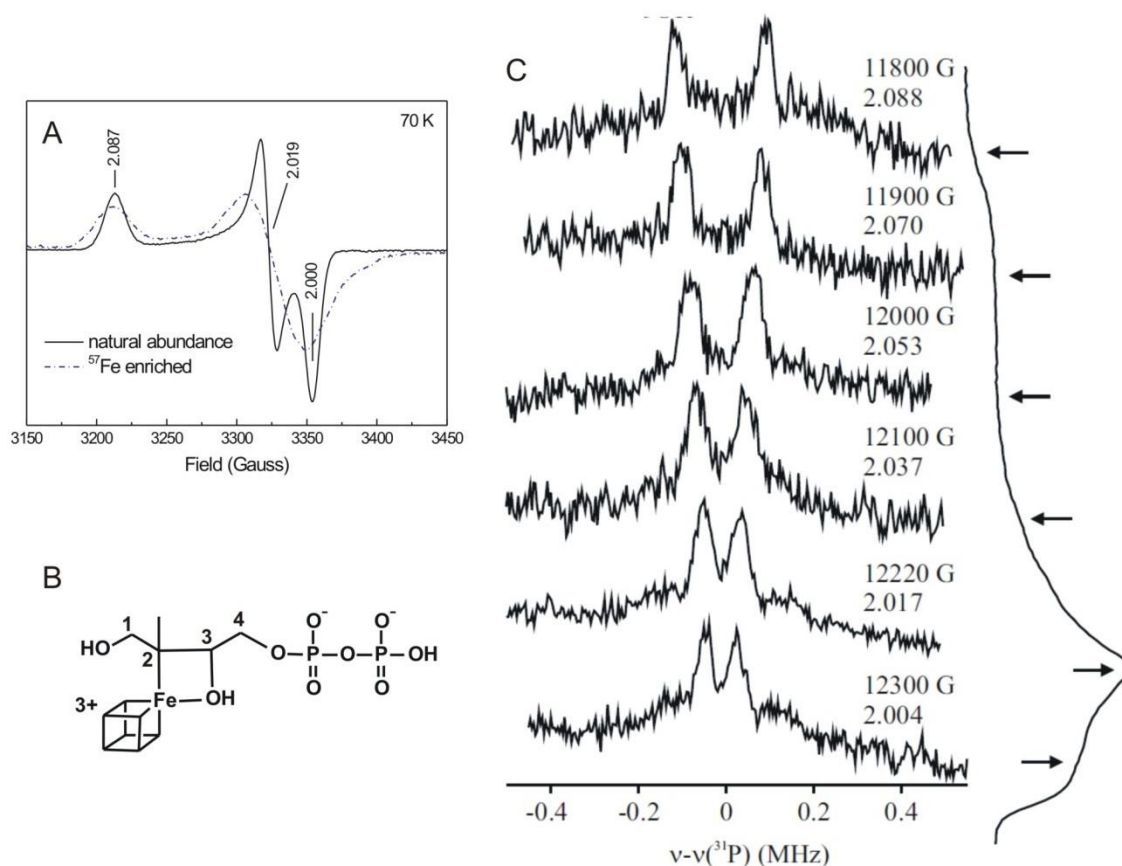
Fig. 34: Panel A; EPR spectrum obtained for GcpE upon incubation with the substrate MEcPP and the reductant dithionite. Panel B: proposed structure for the reaction intermediate. The [4Fe-4S] cluster is represented by the cube. Panel C: ^{13}P-ENDOR spectra. **35 GHz pulsed ^{31}P ENDOR spectra at 2 K.** Spectra were collected at the fields and g values indicated, and are shown alongside the respective pulse-echo detected EPR spectra. ENDOR spectra are normalized to a fixed intensity for clarity.

As an example, let us revisit the IspG enzyme. Figure 35, shows the data obtained using either ^{13}C-MECPP or ^{17}O-labelled HMBPP-epoxide (a substrate analog). The top panel (Panel A) shows the peaks observable due to natural abundance ^{13}C and ^{14}N in the protein sample. In an attempt to study how MEcPP is bound to the cluster, different positions in the MEcPP structure were labeled with either ^{13}C or ^{17}O. Figure 35, panel B, shows the data obtained when both the C3 and the C2 positions are labeled. Now additional peaks show up in the spectrum. The specific assignment is based on a whole set of labeling studies not all shown here. The last panel (panel C), shows the additional peaks observed when the epoxy oxygen of the HMBPP-epoxide is labeled with ^{17}O. The observed interactions are indicative for a short Fe-O bond. The different labeling studies and the obtained data resulted in the binding model shown in Figure 34B.

ENDOR, HYSCORE, and high-frequency EPR are less common techniques and are only available in selected laboratories that are specialized in doing these types of measurements. The technique available at Auburn University is CW X-band EPR spectroscopy. The next chapters will provide information how to run this EPR spectrometer and how to find the correct instrumental settings to get your EPR spectrum. The other techniques are available through collaborations with other labs.

Through these it would be possible to do Q-band and W-band experiments and to obtain ENDOR or HYSCORE data on a particular sample.
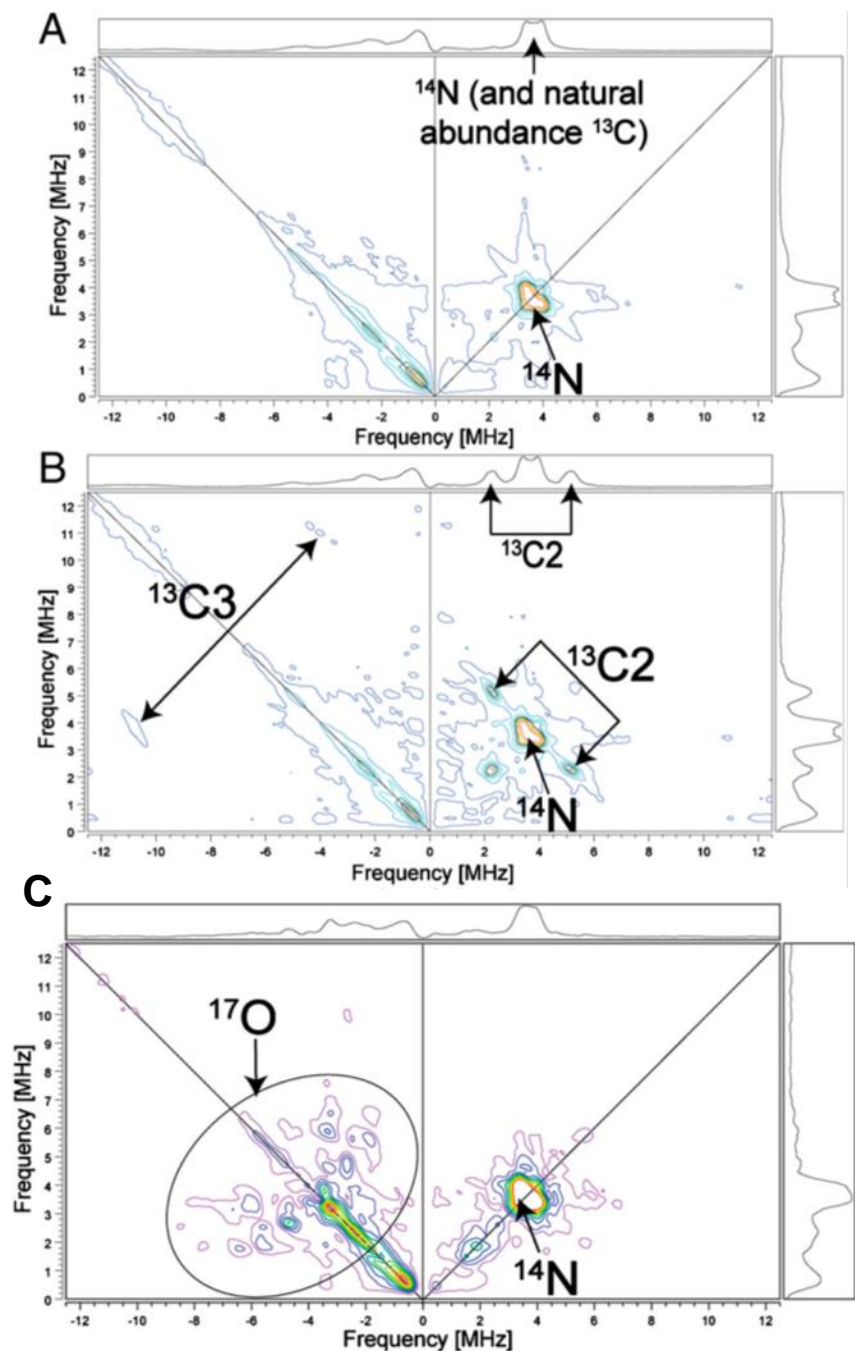

Fig. 35: HYSCORE spectra at g_2 (g = 2.019) of the signal shown in Figure 29. (**A**) GcpE incubated with unlabeled MEcPP. (**B**) As A, but with MEcPP enriched with (∼30%) ^{13}C at C2 and/or C3. (**C**) GcpE incubated with ½ 2;3-[17]O-HMBPP epoxide (as substrate analog). Frequency = 9.64 GHz, spectra were collected at 18 K with τ ¼ 136 ns (Adapted from Wang et al. PNAS 107(2010) 11189).

1.15 Selected reading:

Text Books

1. ***Biomolecular EPR Spectroscopy*** **(2009) Hagen, W.R., CRC Press, Taylor & Francis Group, Boca Raton**

2. *Electron Paramagnetic Resonance: Elementary Theory and Practical Applications* (1994) Weil, J.A., Wertz, J.E. and Bolton, J.R., McGraw-Hill, John Wiley & Co, New York

3. *Principles and Applications of ESR spectroscopy* (2011) Lund, A., Shiotani, M., Shimida, S., Springer, New York

4. *Advanced EPR: Applications in Biology and Biochemistry* (1989) Hoff, A.J. (Ed.), Elsevier, Amsterdam

5. *Principles of Pulse Electron Paramagnetic Resonance* (2001) Schweiger, A., Jeschke, G., Oxford University Press, Oxford

Introductory Articles

6. *Electron Paramagnetic Resonance* (1967) Palmer G., Meth. Enzymol., 10, 594-609

7. *Transition Metal Electron Paramagnetic Resonance Related to Proteins* (1978) Fee, J.A., Meth. Enzymol. 49, 512-528

8. *Electron Paramagnetic Resonance* (1993) Pilbrow, J.R., Hanson, G.R., Meth. Enzymol. 227, 330-353

9. *Electron Paramagnetic Resonance Spectroscopy* (1995) Brudvig, G.W., Meth. Enzymol. 246, 536-554

10. *Protein Structure and Mechanism Studied by Electron Nuclear Double Resonance Spectroscopy* (1995) DeRose, V.J., Hoffman, B.M., Meth. Enzymol. 246, 554-589

11. ***Electron Paramagnetic Resonance of Metalloproteins*** **(2000) Palmer, G., In: Physical Methods in Bioinorganic Chemistry, Que, L., Jr. (Ed.) University Science Books, Sausalito, pp. 121-185**

12. ***ESEEM and ENDOR Spectroscopy*** **(2000) Chasteen, N.D., Snetsinger, P.A., In: Physical Methods in Bioinorganic Chemistry, Que, L., Jr. (Ed.) University Science Books, Sausalito , pp. 187-231**

13. ***EPR Spectroscopy as a Probe of Metal Centres in Biological Systems*** **(2006) Hagen, W.R., Dalton Trans. 4415–4434**

Iron and Iron-Sulfur

14. *EPR Spectroscopy of Components of the Mitochondrial Electron-transfer system* (1978) Beinert, H., *Meth. Enzymol.*, 54, 133-150 (1978)

15. ***Integer-spin Electron Paramagnetic Resonance of Iron Proteins* (1989) Hendrich, M.P., Debrunner, P.G., *Biophys. J.*, 56, 489-506**

16. ***EPR Spectroscopy of Iron-Sulfur Proteins* (1992) Hagen, W.R., *Adv. Inorg. Chem.* 38, 164-222**

17. *Electron Paramagnetic Resonance Spectroscopy of Iron Complexes and Iron-Containing Proteins*, Cammack, R., Cooper, C.E. (1993) *Meth. Enzymol.*, 227, 353-384

18. *Application of EPR Spectroscopy to the Structural and Functional Study of Iron-sulfur Proteins*, Guigliarelli, B., Bertrand, P. (1999) *Adv. Inorg. Chem.*, 47, 421-497

B_{12}

19. *EPR of B_{12}-dependent Enzyme Reactions and Related Systems* (1982) Pilbrow, J.R., In: B_{12}, volume 1, Dolphin, D. (Ed.) John Wiley & Sons, New York, pp. 431-462

20. *EPR Spectroscopy of B_{12}-dependent Enzymes* (1999) Gerfen, G.J., In: Chemistry and Biochemistry of B_{12}, Banerjee R. (Ed.) John Wiley & Sons, New York, pp. 165-195

21. **The positions of radical intermediates in the active sites of adenosylcobalamin-dependent enzymes, Reed, G.H., Mansoorabadi, S.O. (2003) *Curr. Opin. Struct. Biol.* 13, 716-721.**

Other

22. *The Role of Microwave Frequency in EPR Spectroscopy of Copper Complexes* (1982) Hyde, J.S., Froncisz, W., *Ann. Rev. Biophys. Bioeng.* 11, 391-417

23. *Characterization and Reactivity of Surface-localized Inorganic Radicals and Radical Ions* (2010) Chiesa, M., Giamello, E., Che, M., Chem. Rev. 110, 1320-1347